

The impact of resolution on the adjustment and decadal variability of the Atlantic Meridional Overturning Circulation in a coupled climate model

Article

Accepted Version

Paper

Hodson, D. L. R. ORCID: <https://orcid.org/0000-0001-7159-6700> and Sutton, R. T. ORCID: <https://orcid.org/0000-0001-8345-8583> (2012) The impact of resolution on the adjustment and decadal variability of the Atlantic Meridional Overturning Circulation in a coupled climate model. *Climate Dynamics*, 39 (12). pp. 3057-3073. ISSN 1432-0894 doi: <https://doi.org/10.1007/s00382-012-1309-0> Available at <https://centaur.reading.ac.uk/26330/>

It is advisable to refer to the publisher's version if you intend to cite from the work. See [Guidance on citing](#).

To link to this article DOI: <http://dx.doi.org/10.1007/s00382-012-1309-0>

Publisher: Springer

Publisher statement: The original publication is available at www.springerlink.com

All outputs in CentAUR are protected by Intellectual Property Rights law, including copyright law. Copyright and IPR is retained by the creators or other copyright holders. Terms and conditions for use of this material are defined in the [End User Agreement](#).

www.reading.ac.uk/centaur

CentAUR

Central Archive at the University of Reading

Reading's research outputs online

1 **The impact of resolution on the adjustment and decadal**
2 **variability of the Atlantic Meridional Overturning Circulation**
3 **in a coupled climate model**

4 **Daniel L.R. Hodson · Rowan T. Sutton.**

5
6 Received: date / Accepted: date

7 **Abstract** Variations in the Atlantic Meridional Overturning Circulation (MOC) exert an
8 important influence on climate, particularly on decadal time scales. Simulation of the MOC
9 in coupled climate models is compromised, to a degree that is unknown, by their lack of
10 fidelity in resolving some of the key processes involved. There is an overarching need to
11 increase the resolution and fidelity of climate models, but also to assess how increases in
12 resolution influence the simulation of key phenomena such as the MOC.

13 In this study we investigate the impact of significantly increasing the (ocean and atmo-
14 sphere) resolution of a coupled climate model on the simulation of MOC variability by com-
15 paring high and low resolution versions of the same model. In both versions, decadal vari-
16 ability of the MOC is closely linked to density anomalies that propagate from the Labrador
17 Sea southward along the deep western boundary. We demonstrate that the MOC adjustment
18 proceeds more rapidly in the higher resolution model due the increased speed of western
19 boundary waves. However, the response of the Atlantic Sea Surface Temperatures (SSTs) to
20 MOC variations is relatively robust - in pattern if not in magnitude - across the two resolu-
21 tions. The MOC also excites a coupled ocean-atmosphere response in the tropical Atlantic
22 in both model versions. In the higher resolution model, but not the lower resolution model,
23 there is evidence of a significant response in the extratropical atmosphere over the North
24 Atlantic 6 years after a maximum in the MOC. In both models there is evidence of a weak
25 negative feedback on deep density anomalies in the Labrador Sea, and hence on the MOC
26 (with a time scale of approximately ten years). Our results highlight the need for further
27 work to understand the decadal variability of the MOC and its simulation in climate models.

28 **Keywords** Atlantic · MOC · Decadal

D.L.R. Hodson
NCAS-Climate, Department of Meteorology
University of Reading, Earley Gate, PO Box 243
Reading, RG6 6BB, UK
Tel.: +44 118 378 7901
E-mail: d.l.r.hodson@reading.ac.uk

29 1 Introduction

30 The Atlantic Meridional Overturning Circulation (MOC) is responsible for a significant
31 fraction of the meridional heat transport from the tropics to higher latitudes ($\sim 1PW$ at 26N;
32 Biastoch et al (2008), Wunsch and Heimbach (2006), Trenberth and Caron (2001)). Studies
33 suggest that the variability in this transport modulates climate, particularly at northern lat-
34 itudes (e.g. Vellinga et al (2002), Broecker et al (1992)). Although observational estimates
35 of the time mean MOC have been made (Wunsch and Heimbach (2006)), knowledge of its
36 time variations has been hampered by a lack of extended records of subsurface data. Con-
37 tinual monitoring of MOC variability is now underway (Bryden et al (2009), Hirschi et al
38 (2003)), but it will be some decades before enough data is available to infer directly from
39 observations the role of MOC variations in modulating climate.

40 Numerical climate models provide an important alternative source of information for as-
41 sessing the nature and potential climate impacts of MOC variability. Climate models suggest
42 that MOC variations have substantial impacts on climate. For example, northern latitudes
43 cool by $\sim 2K$ following a suppression of the MOC (Vellinga et al (2002), Smith and Gre-
44 gory (2009)), and MOC variations lead to variations in North and South Atlantic Sea Surface
45 Temperatures (SSTs) (Knight et al (2005)). These SST variations can be linked in turn to
46 changes in the seasonal position of the ITCZ, and hence Sahel and South American rainfall
47 (Knight et al (2006), Hodson et al (2009)), in surface air temperatures (Knight et al (2006),
48 Sutton and Hodson (2005)), and in a number of factors controlling Atlantic hurricane gen-
49 esis in models (Knight et al (2006), Sutton and Hodson (2007), Goldenberg et al (2001)).
50 Models also show that variability in the MOC can arise on timescales ranging from days to
51 centuries (e.g. Knight et al (2005), Fanning and Weaver (1998), Dong and Sutton (2005)).
52 The longer timescales are set by oceanic adjustment processes, which are slow compared to
53 those of the atmosphere. Such long adjustment timescales suggest the potential to predict
54 the MOC and its impacts (e.g. Hawkins and Sutton (2008)); consequently, understanding
55 the decadal variability of the MOC is a key issue for ongoing efforts in Decadal Climate
56 Prediction (Smith et al (2007), Keenlyside et al (2008), Pohlmann et al (2009)).

57 One of the challenges for understanding decadal variability of the MOC is that the mag-
58 nitude and dominant time scale of MOC variability has been found to vary substantially
59 between models. These differences arise because of differences in model formulation, but
60 the exact causes can be hard to pinpoint because of the large range of processes involved.
61 A related issue is the modest spatial resolution of current coupled models (typically ~ 1 de-
62 gree in the ocean, and a few degrees in the atmosphere). At such resolutions some of the
63 key processes that are known to influence MOC variability are poorly, or very poorly, re-
64 solved. This weakness inevitably calls into question the relevance of the model results to
65 understanding MOC variability in the real world. Indeed, there is a widespread recognition
66 of the need to increase the resolution of climate models, in order to improve the fidelity with
67 which they simulate the numerous processes that influence climate and climate variability
68 (Shaffrey et al (2009)).

69 Motivated by these issues, the goal of this study is to investigate the simulation of MOC
70 variability in two climate models which differ in resolution, in both the ocean and atmo-
71 sphere. Our aims are to identify the extent to which these models exhibit similar or differing
72 MOC variability, and to seek to understand the reasons for any differences in terms of sim-
73 ulation of the underlying ocean and ocean-atmosphere processes.

74 There are many reasons to expect that the simulation of MOC variability may be sen-
75 sitive to resolution. Interannual and lower frequency variability in the MOC arises primar-
76 ily from two processes: Ekman transport - driven directly by the surface wind stress, and

77 geostrophic transport - driven by the West-East pressure gradient across the Atlantic basin
 78 (Hirschi and Marotzke (2007), Balan Sarojini et al (2011)). Multiannual MOC variations
 79 are primarily geostrophic. A key mechanism involves the formation of density and pres-
 80 sure anomalies on the western boundary of the Sub-polar Gyre, in response to variations
 81 in convection (Marshall and Schott (1999), Gerdes and Köberle (1995)). These boundary
 82 anomalies excite baroclinic boundary waves that propagate south along the western bound-
 83 ary, along the equator and then north and south along the eastern boundary, radiating west-
 84 ward propagating Rossby waves as they go (Kawase (1987), Johnson and Marshall (2002),
 85 Roussenov et al (2008)). This simple picture of ocean adjustment is complicated by the pres-
 86 ence of a sloping coastal shelf, and varying degrees of ocean stratification along the bound-
 87 ary, with the consequence that the boundary wave becomes a hybrid between a coastal shelf
 88 wave and a boundary Kelvin wave (Gerdes and Köberle (1995), Shaw and Csanady (1983)).
 89 This primary rapid (\sim years) adjustment by propagation of baroclinic waves is followed by
 90 second, slower (\sim decades), phase of adjustment that occurs due to the self advection of the
 91 deep density anomaly along the coastal boundary at depth (Gerdes and Köberle (1995)).

92 The timescale of the primary adjustment, and hence the timescale of the MOC adjust-
 93 ment, depends on the speed of the boundary waves communicating the presence of the ad-
 94 justment. Studies have shown that the speed of boundary Kelvin waves is sensitive to model
 95 resolution, and related aspects of model formulation. For example, for a viscous fluid repre-
 96 sented on a Arakawa B-grid, the along-shore phase speed¹ of a Kelvin wave falls rapidly as
 97 grid spacing increases beyond the Rossby radius (Hsieh et al (1983)). When the grid spac-
 98 ing is ten Rossby radii the Kelvin wave phase speed is only 20% of the expected continuum
 99 value (for an extensive discussion see Hsieh et al (1983)). Many modern coupled models,
 100 including the two examined in this study, use an Arakawa B-grid in their ocean component.
 101 In addition, the propagation of boundary waves is sensitive to lateral viscosity. Increased
 102 values of viscosity reduce the along-shore phase speed of coastal Kelvin waves (Davey et al
 103 (1983)). In numerical models values are often used that are larger than observed for reasons
 104 of numerical stability (Jochum et al (2008)). A third numerical factor is the orientation of
 105 the coastal boundary relative to the ocean grid: the along-shore Kelvin wave speed falls as
 106 the angle of the coastline to the underlying grid increases (Schwab (1998)).

107 The importance of resolution for simulation of MOC variability in climate models was
 108 underlined by Döscher et al (1994), who demonstrated - using an ocean model - that the
 109 time taken for coastal boundary waves to travel from high latitudes to the equator was dra-
 110 matically reduced as resolution was increased. Several other ocean model studies have high-
 111 lighted similar issues (Hsieh et al (1983), Beckmann et al (1994), Böning et al (1996), Get-
 112 zclaff et al (2005), Hirschi and Stocker (2002), Johnson and Marshall (2002)). However, as
 113 MOC variability is ultimately driven by atmospheric processes, and variations in the MOC
 114 can influence the atmosphere (e.g. Knight et al (2005)), the potential exists for coupled
 115 feedbacks (e.g. Vellinga and Wu (2004)). Hence a complete understanding of MOC vari-
 116 ability can only be arrived at by considering the coupled atmosphere-ocean system. Studies
 117 which examine the impact of resolution in a coupled system are sparse, due to the expense
 118 of performing the required coupled model integrations at varying resolutions. The study by
 119 Fanning and Weaver (1998) addressed this issue using an ocean model coupled to a simple
 120 2d model of the atmosphere, and concluded that the ocean resolution was a key factor in
 121 the generation of decadal scale MOC variability. However, a fuller assessment of the role of
 122 coupled feedbacks requires a 3d model of the atmosphere.

¹ and hence group speed, since Kelvin waves are non-dispersive.

123 In this paper we examine the impact of resolution on the simulation of MOC variabil-
124 ity in a coupled climate model. The structure of the paper is as follows. In section 2 we
125 present the models and integrations used for the study. In section 3, we present an analysis
126 of the MOC variability and related climate signals found in the models. A Summary and
127 Conclusions are presented in section 4.

128 **2 Models and Experiments**

129 **2.1 Models**

130 Two Coupled General Circulation Models (CGCMs) were used in this study: HadGEM1.2
131 and HiGEM1.2. HadGEM1.2 (Johns et al (2006)) is the most recent version of the UK
132 Hadley Centre global coupled general circulation climate model. The atmosphere compo-
133 nent has a resolution of 1.25° latitude by 1.875° longitude with 38 layers in the vertical.
134 The ocean component, based on the Bryan-Cox code (Bryan (1969), Cox (1984)), uses a
135 latitude-longitude Arakawa-B grid with a zonal resolution of 1° and a meridional resolution
136 of 1° between the poles and 30° latitude, increasing smoothly to $1/3^\circ$ at the equator. It has
137 40 unevenly spaced levels in the vertical.

138 HiGEM1.2 (Shaffrey et al (2009)) is a version of HadGEM1.2 with increased horizontal
139 resolution in both the ocean and the atmosphere. The horizontal resolution has been in-
140 creased to 0.83° latitude x 1.25° longitude in the atmosphere and to $1/3^\circ$ x $1/3^\circ$ in the ocean.
141 The vertical resolution is unchanged in both the atmosphere and ocean components. Small
142 changes are made to some of the parameterizations in the atmosphere to improve model
143 stability but otherwise the HiGEM1.2 atmosphere is identical to that of HadGEM1.2, aside
144 from the change in resolution. The ocean component in HiGEM1.2 is also similarly identi-
145 cal to HadGEM1.2 except that, due to the increased resolution, the Gent-McWilliams (GM
146 - Gent and McWilliams (1990)) adiabatic mixing scheme used in HadGEM1.2 is switched
147 off. The higher horizontal resolution of HiGEM permits partial representation of ocean ed-
148 dies. Tests showed that the inclusion of the GM scheme in HiGEM caused low eddy vari-
149 ability and erosion of fronts. An adiabatic biharmonic scheme is used to reduce tracer field
150 noise. These choices hence preserve ocean features resolvable by the improved resolution. A
151 greater discussion of this and other model differences can be found in Shaffrey et al (2009).

152 **2.2 Experiments**

153 100 year control integrations were performed with both HadGEM1.2 and HiGEM1.2. The
154 ocean initial conditions were formed using September potential temperatures and salinities
155 from the $1/4^\circ$ World Ocean Atlas 2001 (Conkright et al (2002)), with initial velocities set to
156 zero (ocean at rest). Greenhouse gas levels were constant throughout the integrations and
157 identical between the models. Both models reproduce realistic global climates, although
158 there are significant biases (Shaffrey et al (2009)). The climatologies of HiGEM1.2 and
159 HadGEM1.2 control runs are similar, but there are differences, notably HadGEM1.2 SSTs
160 are generally cooler than HiGEM1.2 across the globe. However, oceanic northward heat
161 transports in both models are broadly consistent with the observational estimates. For more
162 details see Shaffrey et al (2009).

163 3 Adjustment and variability of the Atlantic Meridional Overturning Circulation

164 In this section we first examine and contrast basic properties of the mean state and variability
165 of the Atlantic Meridional Overturning Circulation in HiGEM1.2 and HadGEM1.2. We then
166 proceed to examine the drivers and time evolution of the MOC, and its interactions with the
167 atmosphere, in detail.

168 The mean MOCs in HiGEM1.2 and HadGEM1.2 are similar in structure and magni-
169 tude (Figures 1a and b). The overturning cell in HadGEM1.2 is somewhat stronger and the
170 Antarctic Bottom Water (AABW) cell somewhat weaker than HiGEM1.2, although these
171 differences may not be significant compared to year-to-year variability. Both models dis-
172 play an initial very rapid (~ 1 year) reduction in the MOC (HadGEM1.2: 5 Sv, HiGEM1.2:
173 10Sv), probably in response to unbalanced initialization, followed by a slower spin-up re-
174 adjustment over at least the first 30 years (Figures 1c and d). After this period, there is a
175 considerable amount of multi-year variability (Figure 1c). Both models have a mean over-
176 turning (years 31:100, at 26.7N) (HiGEM1.2: 17.8 Sv, HadGEM1.2: 19.6 Sv) in line with
177 the recent observational estimate of 18.7 ± 5.6 Sv (Cunningham et al (2007)).

178 Figures 1c and d show that the overturning at 40N and 26.7N (the latitude of the over-
179 turning estimate presented in Cunningham et al (2007)) is generally consistent across lati-
180 tudes over time within a given model. After the initial 30 year adjustment, there is coherence
181 in the overturning between latitudes on decadal timescales (Figure 2) - as seen in other stud-
182 ies (e.g Balan Sarojini et al (2011)). The tilted contours in both models suggest that changes
183 in the overturning take some time to propagate southwards from their northern source, in
184 a similar manner as seen by Getzlaff et al (2005). There is a possibility that the amplitude
185 of the southward propagating signal is more damped in HadGEM1.2 than HiGEM1.2. The
186 larger amplitude decadal variations in the over-turning are generally found north of 30N. We
187 now concentrate our analysis on the drivers and impacts of these larger variations by focus-
188 ing on variations in the MOC at 40N, the approximate latitude of the maximum meridional
189 stream function in both models (Fig. 1).

190 Interannual-to-decadal variability in the MOC is substantially driven by dense water
191 anomalies that originate from deep-convection regions in the Labrador and GIN seas (Frankig-
192 noul et al (2009), Eden and Willebrand (2001a), Biastoch et al (2008)). Intense surface cool-
193 ing creates dense surface water which sinks through the less-dense sub-layer, leading to a
194 downward mass flux that drives the overturning. Deep mixed layer depths are a signature of
195 deep convection. Peak (March) mixed layer depths in HiGEM1.2 occur principally over the
196 Labrador Sea (50W,55N) and the northern GIN seas (Figure 3a). Convection sites are similar
197 in HadGEM1.2 : the Labrador Sea and the northern GIN seas (Figure 3b). However mixed
198 layer depths are considerably deeper off the coast of Norway and between Scotland and
199 Iceland than are seen in climatological estimates (de Boyer Montégut (2004)). Despite such
200 differences in the March mean mixed layer depth, the patterns of March variability are more
201 consistent between the models (Figures 3c and d) being mostly confined to convection sites
202 in the Labrador Sea and the Northern GIN seas. This suggests that, although there are dif-
203 ferences in the mean convection, the magnitude of the variability - ultimately the driver for
204 MOC variability - is consistent between the models. Both models have distinct convection
205 sites in the Labrador and GIN seas but comparatively little convection in the Irminger sea.
206 Climate models disagree on the relative importance of these sites in driving the overturning
207 (Frankignoul et al (2009), Eden and Willebrand (2001a)).

208 The processes by which dense water anomalies generated by deep convection are com-
209 municated to the wider Atlantic Ocean are complex and not fully understood (Palter et al
210 (2008)). Partly this occurs via interior ocean pathways (Bower et al (2009)), and partly

211 through the propagation of density signals along the western boundary (e.g. Gerdes and
 212 Köberle (1995)). The latter signals are particularly important for the MOC because they
 213 project directly onto the cross-basin zonal density contrast that controls the geostrophic
 214 northward flow.

215 We now examine the propagation of density anomalies that exit the Labrador Sea along
 216 the Deep Western Boundary. Figure 4a shows HiGEM1.2 annual mean depth integrated
 217 (1500:3000m) ocean density correlated with a point on the western boundary (point B, at
 218 40N). There is a very narrow band of high correlations ($\text{corr} > 0.7$) along the western bound-
 219 ary of the North Atlantic, extending from the southern tip of Greenland to the northern coast
 220 of South America. Such a high correlation over an extended region implies a rapidly prop-
 221 agating signal connecting distant points and this is most likely communicated by a rapid
 222 boundary wave response. This boundary wave response is likely to be a mixed Kelvin-
 223 Shelf wave (Gerdes and Köberle (1995)). There are widespread correlations throughout the
 224 Labrador sea, demonstrating that the Labrador sea is a major source of density variations on
 225 the western boundary at depth in HiGEM1.2.

226 Similar high correlations along the western boundary are also found in HadGEM1.2
 227 (Figure 4d), although the correlations in the Labrador sea are much weaker. This difference
 228 reflects a difference between the models in the timescales for density anomalies to propagate
 229 out of the Labrador basin (see Figures 5 and 6, to be discussed shortly).

Density anomalies at the western boundary cause changes in pressure, and hence changes
 in the west-east pressure gradient which drive changes in the MOC. We can examine this re-
 lation between the overturning and the ocean density on the boundaries by following Hirschi
 and Marotzke (2007). Thermal wind balance states that:

$$f \frac{\partial v}{\partial z} = -\frac{g}{\rho^*} \frac{\partial \rho}{\partial x} \quad (1)$$

where $v(x, y, z, t)$ is the meridional ocean velocity, ρ ocean density, ρ^* a reference density,
 f the Coriolis parameter and g the acceleration due to gravity. Integrating across the ocean
 basin, from west (x_w) to east (x_e) and over z from the ocean floor ($z = D$) up to z gives:

$$\int_{x_w}^{x_e} (v(z) - v(D)) dx = -\frac{g}{f\rho^*} \int_D^z (\rho_e - \rho_w) dz \quad (2)$$

where ρ_e (ρ_w) is the density on the Eastern (Western) ocean boundary. Integrating over z
 again:

$$\int_D^z \int_{x_w}^{x_e} (v(z) - v(D)) dx dz = -\frac{g}{f\rho^*} \int_D^z \int_D^z (\rho_e - \rho_w) dz dz \quad (3)$$

We now follow Hirschi and Marotzke (2007) and assume that the bottom ocean velocities
 are zero ($v(D) = 0$). The left hand side of (3) is hence the volume flux below a depth z , i.e.
 the stream function $\Psi(z)$ or overturning. Hence the volume flux is proportional to the double
 integral of the boundary density difference. For the remainder of this paper we make two
 further assumptions. i) Variations over time in the density contrast on the right hand side
 of (3) are dominated by ρ_w - this is likely to be true because of greater density variations
 along the western boundary that are not present on the eastern boundary. ii) Variations in
 the volume flux below 1000m are dominated by the region between 1500m and 3000m.
 This region captures the depths of maximum southward flow and excludes variations in the
 Antarctic Bottom Water (Figure 1). Hence (3) can be reduced to:

$$\Psi(1000) \approx \frac{g}{f\rho^*} \int_{3000}^{1500} \int (\rho_w) d^2z \quad (4)$$

Figure 4b demonstrates that in HiGEM1.2 (at 40N) variations in (4) are indeed well correlated with the overturning at 40N (corr = 0.6). Interestingly, the overturning is almost identically correlated with the single integral of the density on the boundary (corr = 0.57). That is:

$$MOC^* \propto \int_{3000}^{1500} (\rho_w) dz \quad (5)$$

This relationship appears to hold in both HiGEM1.2 and HadGEM1.2 (figure 4). MOC^* and the overturning are well correlated at 40N but they are less well correlated further south at 27N, the latitude of the RAPID array (Figure 4c, corr = 0.40). This may be due to increased influence of wind driven (Ekman) transport variability at this latitude, or the failure of one of our assumptions in the derivation of (4). In HadGEM1.2, The correlation between the boundary density and the MOC is greater than HiGEM1.2 (Figure 4e and f), most likely due to the presence of the larger amplitude decadal signal in HadGEM1.2. The correlations between the boundary density and the MOC are similarly stronger at 40N (corr = 0.80) than 26.7N (corr = 0.38) in HadGEM1.2.

It is apparent from Figure 4 that the correlation between MOC^* and the actual overturning is particularly high on decadal timescales. This is partly because MOC^* filters out the Ekman contribution to MOC variability that is large on interannual (and shorter) time scales, but is of relatively little interest from a climatic point of view. For this reason, for the remainder of this paper we will use MOC^* at 40N, as our measure of MOC variability. Hence we are focusing on that component of the MOC variability that is directly related to variations in the density on the deep western boundary.

3.1 Ocean Adjustment

We now examine the temporal evolution of the boundary density anomaly that controls the MOC adjustment. Figure 5 shows the 1500-3000m integrated density lag-regressed onto MOC^* at 40N in HiGEM1.2. Positive density anomalies are seen in the Labrador Sea four years prior to a maximum in MOC^* (panel a). Subsequent lags show a boundary density signal propagating out of the Labrador Sea, along the western boundary (panels b, c, d). When this signal reaches the equator it triggers a tropical response that is consistent with theoretical expectations and other studies (e.g. Johnson and Marshall (2002)). The tropical response is governed by the excitation of an eastward propagating equatorial Kelvin wave, which subsequently excites coastal Kelvin waves on the eastern boundary, which then radiate westward propagating Rossby waves. This signal is weak ($p < 0.10$), but clear at Lags 0 and 2. These signals subsequently decay (panels e, f). In addition to the western boundary signal, density anomalies are seen to propagate southward into the interior of the basin, in a manner consistent with recent observations (Bower et al (2009)) (Figure 5d, e, f). Lastly, there is an interesting hint in panel f of *negative* density anomalies around the boundary of the Labrador Sea. These negative anomalies appear 6 years after a maximum in the MOC^* and could suggest a negative feedback on MOC variations.

A similar picture emerges for HadGEM1.2 (Figure 6). Density anomalies propagate out of the Labrador basin and around the western boundary (panels a-d) - although the boundary density signal is less tightly confined to the western boundary than the HiGEM1.2 signal - and finally across the equator (at Lag 2), in the manner described above.

The equatorial Kelvin-wave response occurs somewhat earlier in HiGEM1.2 (Lag 0 years) than HadGEM1.2 (Lag 2 years). This suggests that density anomalies may take longer to propagate along the western boundary to the equator in HadGEM1.2 than in HiGEM1.2.

270 As noted in the introduction, it is well-known that boundary wave propagation speeds
271 on Arakawa-B grids are sensitive to model resolution (Hsieh et al (1983)). Both oceans
272 models in HiGEM1.2 and HadGEM1.2 are discretized on Arakawa-B grids (Johns et al
273 (2006), Shaffrey et al (2009)) so it is likely that the different timescales for propagation of
274 the boundary density waves between the models can be attributed to the differences in ocean
275 model resolution. Indeed examining the variation of the Rossby radius of deformation within
276 the Atlantic (Chelton et al (1998)) reveals that boundary density waves are not well resolved
277 in HadGEM1.2 north of 10N whereas they are resolved in HiGEM1.2 south of around 30N.
278 Hence we expect that the propagation speed of boundary waves in HadGEM1.2 will differ
279 from that in HiGEM1.2 between 10N and 30N.

280 In other respects, the ocean evolution in HadGEM1.2 is similar to that in HiGEM1.2 .
281 HadGEM1.2 displays propagation of Labrador Sea density anomalies into the basin interior,
282 and also a negative density anomaly in the Labrador Sea at lag 6 (Figure 6f).

283 3.2 Atmosphere-Ocean Interactions

284 We now turn our attention to the interaction of MOC variability with the overlying atmo-
285 sphere. Figures 7 and 8 show lagged regressions of Mean Sea Level Pressure (MSLP) onto
286 MOC^* at 40N for the two models. We focus first on negative lags, which may provide evi-
287 dence of the atmospheric forcing of MOC variability. In HiGEM1.2 strong negative MSLP
288 anomalies are found over Greenland 2-4 years before a maximum in MOC^* (Figure 7a and
289 b). The pressure gradients associated with these anomalies will induce anomalous south-
290 ward (northerly) winds over the Labrador Sea, advecting cold air over the region, resulting
291 in intense cooling. This cooling is clearly seen in the surface heat fluxes over the Labrador
292 Sea at these lags (not shown). Hence in HiGEM1.2 dense Labrador Sea water, generated by
293 wind-driven surface cooling, subsequently induces changes in the MOC. This is consistent
294 with many previous studies (Dickson et al (1996), Curry et al (1998), Eden and Willebrand
295 (2001a), Bentsen et al (2004), Guemas and Salas-Méllia (2008)).

296 In contrast to HiGEM1.2, in HadGEM1.2 there is little evidence of significant and coher-
297 ent MSLP anomalies over the North Atlantic at negative lags (Figures 8a, b). (Such signals
298 are also not found at more negative lags (not shown)). This suggests that the large amplitude
299 decadal fluctuations in the MOC^* in HadGEM1.2 (figures 4e and f) are not directly forced
300 by the atmosphere over the North Atlantic. They may, for example, originate from ocean
301 density anomalies propagating out of the Arctic.

302 Next we consider positive lags, which may provide evidence of an atmospheric response
303 to MOC variability. To aid the interpretation of these signals we also need to examine the
304 regression patterns for sea surface temperature (SST) on MOC^* (Figure 9). The SST pattern
305 for HiGEM1.2 at lag 0 (panel a) shows cool (negative) anomalies over the Labrador Sea,
306 as expected in response to the cooling by surface heat fluxes over the preceding years (see
307 e.g. Eden and Willebrand (2001a) etc). Warm (positive) anomalies are also seen over the
308 Gulf Stream extension and North Atlantic Current region. Over subsequent years (panels
309 b and c), this warm anomaly appears to propagate northwards into the eastern part of the
310 sub-polar gyre, whilst the cool anomalies over the western sub-polar gyre decay. By lag 6,
311 warm anomalies cover the sub-polar gyre and are also linked along the eastern boundary to
312 a warm anomaly in the tropical North Atlantic. A small cool anomaly is found in the region
313 of the Gulf Stream extension. Similar negative anomalies have been linked to a southward
314 displacement of the Gulf Stream front related to variability in the MOC (Zhang (2008)).

315 The evolution of MSLP at positive lags in HiGEM1.2 (Figure 7e,f) shows initially the
316 appearance of a low pressure anomaly over the tropical Atlantic, and subsequently - at lag
317 6 - a dipolar pattern with a high pressure anomaly centred over Greenland and a low pres-
318 sure anomaly over the mid-latitude North Atlantic. This MSLP pattern is associated with
319 a weakening of the westerlies that are closely linked with the North Atlantic storm track.
320 Inspection of the SST pattern at this time (Figure 9c) shows a weakening of the meridional
321 SST gradient east of Newfoundland. Such a weakening of the SST gradient would be ex-
322 pected to weaken the storm track, and may provide a mechanism for the excitation of a
323 large-scale atmospheric response, as suggested by Figure 7f. Additionally, this may also be
324 a remote response to the developing Tropical Atlantic SST warm anomaly (see e.g. Terray
325 and Cassou (2002), Dréevillon et al (2003) and Cassou et al (2004)).

326 The evolution of SST in HadGEM1.2 (Figure 9d-f) shows some similar features to
327 HiGEM1.2 but the anomalies are of greater magnitude. At lag 0, a warm anomaly is again
328 seen in the region of the North Atlantic Current, and this anomaly subsequently appears
329 to propagate into the sub-polar gyre, concurrent with the development of a linked warm
330 anomaly in the tropical North Atlantic. Significant warm tropical SST anomalies appear
331 earlier in HadGEM and are linked with cool (negative) SST anomalies south of the equator
332 (and hence a cross-equator SST gradient). A (very) small cool SST anomaly is also found
333 at lag 6 in the region of the Gulf Stream extension. The evolution of MSLP (Figure 8d,e,f)
334 shows the development of a low pressure anomaly over the tropical North Atlantic, with
335 peak intensity at lag 4 (when a similar signal was seen in HiGEM1.2). There are no strong
336 anomalies in MSLP over the higher latitude North Atlantic in HadGEM1.2. Large anom-
337 alies are present over the North Pacific but it is unclear whether these are causally linked to
338 the variability in the Atlantic basin.

339 In both models significant anomalies in both MSLP and SST develop in the tropical
340 North Atlantic. The tropical Atlantic is a region of strong ocean-atmosphere coupling, where
341 - moreover - coupled feedbacks, particularly related to the cross-equator SST gradient, can
342 act to amplify initially small anomalies (e.g. Chang et al (1997), Sutton et al (2000)). There
343 is evidence of these feedbacks operating in both HadGEM1.2 and HiGEM1.2. Figure 11
344 shows the surface wind stress and wind speed anomalies at lag 6 in the two models. In
345 both cases there is cross-equator flow, as expected in response to the cross-equator SST
346 gradient. Furthermore, the variations in wind speed magnitude and direction are consistent
347 with turbulent (latent and sensible) surface heat flux anomalies that will act to reinforce the
348 anomalous SSTs both north and south of the equator. Note that there is also an associated
349 northward displacement of the ITCZ (not shown).

350 An interesting question concerning the tropical response is whether it is linked in any
351 way to the deep density signal propagating along the western boundary (Figure 5 and Fig-
352 ure 6). Examining the vertical structure of temperature anomalies in the tropical North At-
353 lantic at lag 6 (Figure 10a & b) shows a deep sub-surface negative temperature anomaly in
354 HadGEM1.2 that is related to the high density anomaly seen in Figure 6f. A similar but much
355 weaker anomaly can be seen in HiGEM1.2. In both cases, however, the deep anomalies are
356 much weaker than those near the surface, and show no obvious connection to them. Rather
357 it appears that the near surface anomalies can be more readily understood as a response to
358 the surface wind anomalies (Figure 11). This response involves anomalous turbulent heat
359 fluxes, as previously mentioned, and also - particularly within $\sim 5^\circ$ of the Equator - anom-
360 alies in Ekman pumping. Figure 11d indicates downward Ekman pumping near the Equator
361 in HadGEM1.2, which acts to deepen the thermocline. This influence explains the presence
362 of a warm temperature anomaly beneath the cool SST anomalies in the tropical South At-

363 lantic (Figure 10d) and the warm subsurface temperature anomalies in the tropical North
364 Atlantic (Figure 10c).

365 Although the upper ocean response appears to be dominated by the influence of the
366 atmosphere, and related coupled feedbacks, it is still possible that the density signals prop-
367 agating along the western boundary might provide an initial trigger for the development
368 of tropical SST anomalies that subsequently amplify through coupled feedbacks. One way
369 in which this might happen is through a modulation of the North Brazil Current (NBC)
370 (e.g. Zhang et al (2011)) and its subsequent effects on SST. To investigate this question we
371 correlated various indices of the NBC with MOC^* . Figure 12 shows results for an NBC
372 index, defined as the meridional northward ocean velocity integrated over the top 100m
373 in the ocean and then averaged over the region (60W:45W,2N:10N) and then detrended. Whilst
374 the correlations are weak, in the case of HadGEM1.2 significant correlations are found for
375 lags between 0 and 6 years following a maximum in MOC^* . This link between a MOC^*
376 maximum and an acceleration of the NBC may be mediated by the baroclinic coastal Kelvin
377 waves that follow a MOC^* maximum. It might also be mediated by the wind stress anom-
378 alies that develop over the tropical Atlantic (Figure 11) or a number of other mechanisms
379 (see Zhang et al (2011)). However, the fact that the correlation in Fig 12a starts to increase
380 rapidly around 4 years before a maximum in the MOC^* (i.e. Lag -4), before significant wind
381 anomalies have developed, suggests the deep density signal may indeed play a triggering
382 role. This does not provide conclusive evidence of a causal oceanic connection, but does
383 suggest such a connection may exist. In HiGEM1.2, the evidence is weaker.

384 If the deep density signals do not provide the initial trigger for development of the trop-
385 ical anomalies, what other mechanisms might? One possibility is an atmospheric telecon-
386 nection from the higher latitude North Atlantic. Extratropical forcing of the tropical Atlantic
387 has been demonstrated in several recent modelling studies (Broccoli et al (2006) and Zhang
388 et al (2010), Kang et al (2009)). Another possibility is an oceanic teleconnection via ad-
389 vection of SST anomalies from the Gulf Stream region southward around the subtropical
390 gyre and into the tropics. The pattern of SST anomalies seen in HiGEM1.2 at lag 6 (Figure
391 9b) is possibly suggestive of this mechanism, but it perhaps unlikely that this is a dominant
392 factor, in view of the tendency for midlatitude SST anomalies to be damped unless main-
393 tained by strong circulation anomalies. Also, the timescale of propagation seen appears to
394 be faster than those that could be supported by passive advection by a climatological ocean
395 circulation.

396 A last point of interest is the hints from Figures 5 and 6 of a negative feedback on
397 deep density in the Labrador Sea, with negative anomalies following positive anomalies by
398 around 10 years in both HiGEM1.2 and HadGEM1.2. The signals are weak and should not
399 be over-interpreted, but the consistency between the models is interesting and could suggest
400 a robust mechanism. What might this mechanism be? A simple possibility is suggested by
401 Figure 9c,f. This figure shows that the appearance of negative density anomalies at depth
402 in the Labrador Sea follows, and coincides with, the warming of SST over the whole sub-
403 polar gyre, including the Labrador Sea. This warming will tend to increase stratification and
404 inhibit the tendency of wintertime convection to cool the subsurface ocean. Therefore we
405 tentatively hypothesise that the negative feedback arises from the northward propagation of
406 the warming signal from the North Atlantic Current region into the sub-polar gyre, asso-
407 ciated with a peak in the MOC. Note that this evolution is very similar to that which was
408 observed in the real world during the mid-1990s (Robson et al (2011)).

409 4 Summary and Conclusions

410 In this paper we have examined the adjustment and decadal variability of the Atlantic
411 Meridional Overturning Circulation (MOC) in two coupled climate models, which differ
412 only in respect of resolution. The two models - HiGEM1.2 (high horizontal resolution) and
413 HadGEM1.2 (standard horizontal resolution) - were integrated using identical initial and
414 boundary conditions. We then examined and compared the evolution of the MOC, and its
415 interactions with the atmosphere, in each model. The major findings are as follows:

- 416 – In both HiGEM1.2 and HadGEM1.2, decadal variability of the MOC is very closely
417 tied to variability in density along the deep western boundary of the Atlantic Ocean.
418 Density anomalies formed in the Labrador Sea propagate southwards along the western
419 boundary and into the tropics, consistent with theory and much simpler models (e.g.
420 Johnson and Marshall (2002)). Density anomalies also propagate into the interior of the
421 North Atlantic basin, consistent with observations (Bower et al (2009)).
- 422 – In HiGEM1.2, density anomalies in the Labrador Sea appear to be generated in re-
423 sponse to atmospheric variations that modulate air-sea fluxes, consistent with many
424 other studies (e.g. Eden and Willebrand (2001b), Köhl (2005)). Such a link is not seen
425 in HadGEM1.2.
- 426 – Both models respond to Labrador Sea density anomalies in a similar way but the time
427 taken for the anomalies to propagate to the equator differs. HadGEM1.2 adjusts more
428 slowly (by 1-2 years) than HiGEM1.2. This difference is attributed to slower western
429 boundary waves in HadGEM1.2, which are expected as a consequence of the lower
430 horizontal resolution (Hsieh et al (1983)).
- 431 – Despite this difference in the adjustment timescale of the deep ocean, the North Atlantic
432 SST anomalies that are related to the MOC evolve in a similar manner in the two models.
433 The magnitude of SST anomalies is larger in HadGEM1.2 than in HiGEM1.2, but in
434 both cases warm anomalies are first seen in the region of the Gulf Stream Extension /
435 North Atlantic Current, and subsequently spread throughout the sub polar gyre and also
436 develop in the tropical North Atlantic.
- 437 – In both models, the tropical SST anomalies are linked to local MSLP anomalies and
438 grow over several years, likely through coupled ocean-atmosphere feedbacks that in-
439 volve the cross-equator SST gradient. Wind anomalies are associated with anomalous
440 surface fluxes that influence SST and also, close to the Equator, anomalous Ekman
441 pumping that influences thermocline depth. The initial trigger for the development of
442 a tropical SST and atmosphere response may arise from an atmospheric teleconnection
443 from the North Atlantic. In the case of HadGEM1.2 there is also evidence of a role for
444 an acceleration of the near surface North Brazil Current, possibly linked to the deep
445 density anomaly that propagates southward from the North Atlantic.
- 446 – In HiGEM1.2 there is evidence of a significant response in the extratropical atmosphere
447 over the North Atlantic 6 years after a maximum in the MOC. A dipolar pattern of
448 MSLP is related to a weakening of the mid-latitude westerlies that may be a response to
449 a weakening of the meridional SST gradient east of Newfoundland. Such a response is
450 not seen in HadGEM1.2.
- 451 – In both models there is evidence of a weak negative feedback on density anomalies in
452 the Labrador Sea, and hence on the MOC. This feedback is related to a warming of the
453 upper sub-polar gyre that increases stratification and is expected to inhibit convection.
454 The time scale for this feedback is approximately 10 years in both models.

455 These results suggest that for climate models, at least with those where the ocean is
456 discretized on an Arakawa B grid, the timescale of deep ocean evolution and adjustment is
457 sensitive to resolution. However, the evolution of SST - a key issue from the perspective of
458 decadal forecasting - appears less affected by resolution in terms of timing and pattern (al-
459 though it is harder to make a firm statement about the magnitude). The response of tropical
460 SST and climate shows important robust features between the two models, but also many
461 detailed differences. Perhaps the most important differences are those seen in the extrat-
462 ropical atmosphere, where the behaviour of the two models appears quite different. Further
463 understanding of these differences will clearly be an important topic for further work.

464 To end we acknowledge some limitations of our study. Firstly, ideally we would have had
465 available longer model simulations and therefore more realisations of decadal fluctuations.
466 Unfortunately the computation cost of the high resolution model precluded this. Secondly,
467 in discussing our results we have assumed implicitly that all the differences are directly
468 attributable to the differences in resolution. Because some modest re-tuning (e.g. to the
469 ocean mixing schemes) was required, this might not be the case. On the other hand, such
470 secondary changes may be considered part of the change in the model resolution, since no
471 stable model would exist without them.

472 We have focused in this paper on two models that use an ocean model based on an
473 Arakawa B-grid ocean. Many other ocean models use the Arakawa-C grid discretization.
474 The C-grid is predicted to be less sensitive to resolution in terms of boundary wave speed
475 (Hsieh et al (1983)). Further experiments will be required to assess whether the behaviour
476 of the MOC is indeed less sensitive to horizontal resolution in climate models that employ
477 a C-grid ocean.

478 It remains the case that the resolution of current climate models places a fundamental
479 limitation on their fidelity. Understanding how increases in resolution influence the simula-
480 tion of mean climate, climate variability and change is a key challenge on which a great deal
481 of further work is required.

482 **Acknowledgements** The Authors would like to thank Len Shaffrey and the HiGEM project for use of the
483 HiGEM and HadGEM data in this study and two anonymous Reviewers for their valuable comments which
484 notably improved the manuscript. This work was funded by the UK National Environment Research Council
485 (NERC) Grant no. NE/F018533/1 and by the NERC NCAS-Climate programme.

486 References

- 487 Balan Sarojini B, Gregory JM, Tailleux R, Bigg GR, Blaker AT, Cameron D, Edwards
488 NR, Megann AP, Shaffrey LC, Sinha B (2011) High frequency variability of the At-
489 lantic meridional overturning circulation. *Ocean Science Discussions* 8(1):219–246 doi:
490 doi:10.5194/osd-8-219-2011
- 491 Böning CW, Bryan FO, Holland WR, Döscher R (1996) Deep-Water Forma-
492 tion and Meridional Overturning in a High-Resolution Model of the North
493 Atlantic. *Journal of Physical Oceanography* 26(7):1142–1164, doi:10.1175/1520-
494 0485(1996)026%3C1142:DWFAMO%3E2.0.CO;2
- 495 Beckmann A, Böning CW, Köberle C, Willebrand J (1994) Effects of Increased Horizontal
496 Resolution in a Simulation of the North Atlantic Ocean. *Journal of Physical Oceanogra-*
497 *phy* 24(2):326–344, doi:10.1175/1520-0485(1994)024%3C0326:EOIHRI%3E2.0.CO;2

- 498 Bentsen M, Drange H, Furevik T, Zhou T (2004) Simulated variability of the Atlantic meridional overturning circulation. *Climate Dynamics* 22(6):701–720, doi:10.1007/s00382-004-0397-x
- 499
- 500
- 501 Biastoch A, Böning CW, Getzlaff J, Molines JM, Madec G (2008) Causes of Interannual Decadal Variability in the Meridional Overturning Circulation of the Midlatitude North Atlantic Ocean. *J Climate* 21(24):6599–6615, doi:10.1175/2008JCLI2404.1
- 502
- 503
- 504 Bower AS, Lozier SM, Gary SF, Boning CW (2009) Interior pathways of the North Atlantic meridional overturning circulation. *Nature* 459(7244):243–247, doi:10.1038/nature07979
- 505
- 506 de Boyer Montégut C (2004) Mixed layer depth over the global ocean: An examination of profile data and a profile-based climatology. *Journal of Geophysical Research* 109(C12), doi:10.1029/2004JC002378
- 507
- 508
- 509 Broccoli AJ, Dahl KA, Stouffer RJ (2006) Response of the ITCZ to Northern Hemisphere cooling. *Geophysical Research Letters* 33(1):L01,702+, doi:10.1029/2005GL024546
- 510
- 511 Broecker W, Bond G, Klas M, Clark E, McManus J (1992) Origin of the northern Atlantic's Heinrich events. *Climate Dynamics* 6(3):265–273, doi:10.1007/BF00193540
- 512
- 513 Bryan K (1969) A numerical method for the study of the circulation of the world ocean. *Journal of Computational Physics* 4(3):347–376, doi:10.1016/0021-9991(69)90004-7
- 514
- 515 Bryden HL, Mujahid A, Cunningham SA, Kanzow T (2009) Adjustment of the basin-scale circulation at 26 N to variations in Gulf Stream, deep western boundary current and Ekman transports as observed by the Rapid array. *Ocean Science Discussions* 6(1):871–908
- 516
- 517
- 518 Cassou C, et al (2004) Summer sea surface temperature conditions in the north atlantic and their impact upon the atmospheric circulation in early winter. *J Climate* 17:3349–3363
- 519
- 520 Chang P, Ji L, Li H (1997) A decadal climate variation in the tropical Atlantic Ocean from thermodynamic air-sea interactions. *Nature* 385(6616):516–518, doi:10.1038/385516a0
- 521
- 522 Chelton DB, deSzoeke RA, Schlax MG, El Naggar K, Siwertz N (1998) Geographical Variability of the First Baroclinic Rossby Radius of Deformation. *Journal of Physical Oceanography* 28(3):433–460, doi:10.1175/1520-0485(1998)028%3C0433:GVOTFB%3E2.0.CO;2
- 523
- 524
- 525
- 526 Conkright ME, Locarnini RA, Garcia HE, O'Brien TD, Boyer TP, Stephen C, Antonov JI (2002) *World Ocean Atlas 2001: Objective Analyses, Data Statistics, and Figures*, CD-ROM Documentation. National Oceanographic Data Center, Internal Rep (17)
- 527
- 528
- 529 Cox MD (1984) A primitive equation, three dimensional model of the ocean. Tech. rep., GFDL, Princeton, NJ
- 530
- 531 Cunningham SA, Kanzow T, Rayner D, Baringer MO, Johns WE, Marotzke J, Longworth HR, Grant EM, Hirschi JJM, Beal LM, Meinen CS, Bryden HL (2007) Temporal variability of the atlantic meridional overturning circulation at 26.5degreesn. *Science* 317(5840):935–938, doi:10.1126/science.1141304
- 532
- 533
- 534
- 535 Curry RG, McCartney MS, Joyce TM (1998) Oceanic transport of subpolar climate signals to mid-depth subtropical waters. *Nature* 391(6667):575–577, doi:10.1038/35356
- 536
- 537 Döschner R, Böning CW, Herrmann P (1994) Response of Circulation and Heat Transport in the North Atlantic to Changes in Thermohaline Forcing in Northern Latitudes: A Model Study. *Journal of Physical Oceanography* 24(11):2306–2320, doi:10.1175/1520-0485(1994)024%3C2306:ROCAHT%3E2.0.CO;2
- 538
- 539
- 540
- 541 Davey MK, Hsieh WW, Wajsowicz RC (1983) The Free Kelvin Wave with Lateral and Vertical Viscosity. *Journal of Physical Oceanography* 13(12):2182–2191, doi:10.1175/1520-0485(1983)013%3C2182:TFKWVL%3E2.0.CO;2
- 542
- 543
- 544 Dickson R, Lazier J, Meincke J, Rhines P, Swift J (1996) Long-term coordinated changes in the convective activity of the North Atlantic. *Progress In Oceanography* 38(3):241–295,
- 545

- doi:10.1016/S0079-6611(97)00002-5
- 546 Dong B, Sutton RT (2005) Mechanism of Interdecadal Thermohaline Circulation Variability
547 in a Coupled Ocean–Atmosphere GCM. *Journal of Climate* 18(8):1117–1135, doi:
548 10.1175/JCLI3328.1
- 549 Dréevillon M, Cassou C, Terray L (2003) Model study of the North Atlantic region at-
550 mospheric response to autumn tropical Atlantic sea-surface-temperature anomalies. *QJR*
551 *Meteorol Soc* 129(593):2591–2611, doi:10.1256/qj.02.17
- 552 Eden C, Willebrand J (2001a) Mechanism of Interannual to Decadal Variability
553 of the North Atlantic Circulation. *J Climate* 14(10):2266–2280, doi:10.1175/1520-
554 0442(2001)014%3C2266:MOITDV%3E2.0.CO;2
- 555 Eden C, Willebrand J (2001b) Mechanism of interannual to decadal variability of the north
556 atlantic circulation. *J Climate* 14(10):2266–2280
- 557 Fanning AF, Weaver AJ (1998) Thermohaline Variability: The Effects of Horizontal
558 Resolution and Diffusion. *Journal of Climate* 11(4):709–715, doi:10.1175/1520-
559 0442(1998)011%3C0709:TVTEOH%3E2.0.CO;2
- 560 Frankignoul C, Deshayes J, Curry R (2009) The role of salinity in the decadal variability of
561 the North Atlantic meridional overturning circulation. *Climate Dynamics* 33(6):777–793,
562 doi:10.1007/s00382-008-0523-2
- 563 Gent PR, McWilliams JC (1990) Isopycnal Mixing in Ocean Circulation Mod-
564 els. *Journal of Physical Oceanography* 20(1):150–155, doi:10.1175/1520-
565 0485(1990)020%3C0150:IMIOCM%3E2.0.CO;2
- 566 Gerdes R, Köberle C (1995) On the Influence of DSOW in a Numerical Model of the North
567 Atlantic General Circulation. *J Phys Oceanogr* 25(11):2624–2642, doi:10.1175/1520-
568 0485(1995)025%3C2624:OTIODI%3E2.0.CO;2
- 569 Getzlaff J, Böning CW, Eden C, Biastoch A (2005) Signal propagation related to the North
570 Atlantic overturning. *Geophysical Research Letters* 21
- 571 Goldenberg SB, Landsea CW, Mestas-Núñez AM, Gray WM (2001) The Recent Increase in
572 Atlantic Hurricane Activity: Causes and Implications. *Science* 293(5529):474–479, doi:
573 10.1126/science.1060040
- 574 Guemas V, Salas-Méllia D (2008) Simulation of the Atlantic meridional overturning circula-
575 tion in an atmosphereocean global coupled model. Part I: a mechanism governing the vari-
576 ability of ocean convection in a preindustrial experiment. *Climate Dynamics* 31(1):29–48,
577 doi:10.1007/s00382-007-0336-8
- 578 Hawkins E, Sutton R (2008) Potential predictability of rapid changes in the Atlantic
579 meridional overturning circulation. *Geophysical Research Letters* 35(11):L11,603+, doi:
580 10.1029/2008GL034059
- 581 Hirschi J, Marotzke J (2007) Reconstructing the Meridional Overturning Circulation from
582 Boundary Densities and the Zonal Wind Stress. *Journal of Physical Oceanography*
583 37(3):743–763, doi:10.1175/JPO3019.1
- 584 Hirschi J, Stocker TF (2002) Rapid changes of the oceanic circulation in a hierarchy of
585 ocean models. *Tellus A* 54(3):273–287, doi:10.1034/j.1600-0870.2002.00323.x
- 586 Hirschi J, Baehr J, Marotzke J, Stark J, Cunningham S, Beismann JO (2003) A monitoring
587 design for the Atlantic meridional overturning circulation. *Geophysical Research Letters*
588 30(7):1413+, doi:10.1029/2002GL016776
- 589 Hodson DLR, Sutton RT, Cassou C, Keenlyside N, Okumura Y, Zhou T (2009) Climate
590 impacts of recent multidecadal changes in Atlantic Ocean Sea Surface Temperature: a
591 multimodel comparison. *Climate Dynamics* doi:10.1007/s00382-009-0571-2
- 592 Hsieh WW, Davey MK, Wajsowicz RC (1983) The Free Kelvin Wave in Finite-
593 Difference Numerical Models. *Journal of Physical Oceanography* 13(8):1383–1397, doi:
594

- 10.1175/1520-0485(1983)013%3C1383:TFKWIF%3E2.0.CO;2
- 595 Jochum M, Danabasoglu G, Holland M, Kwon YO, Large WG (2008) Ocean
596 viscosity and climate. *Journal of Geophysical Research* 113(C6):C06,017+, doi:
597 10.1029/2007JC004515
- 598 Johns TC, Durman CF, Banks HT, Roberts MJ, McLaren AJ, Ridley JK, Senior CA,
599 Williams KD, Jones A, Rickard GJ, Cusack S, Ingram WJ, Crucifix M, Sexton DMH,
600 Joshi MM, Dong BW, Spencer H, Hill RSR, Gregory JM, Keen AB, Pardaens AK, Lowe
601 JA, Bodas-Salcedo A, Stark S, Searl Y (2006) The New Hadley Centre Climate Model
602 (HadGEM1): Evaluation of Coupled Simulations. *Journal of Climate* 19(7):1327–1353,
603 doi:10.1175/JCLI3712.1
- 604 Johnson HL, Marshall DP (2002) A Theory for the Surface Atlantic Response to Thermoha-
605 line Variability. *Journal of Physical Oceanography* 32(4):1121–1132, doi:10.1175/1520-
606 0485(2002)032%3C1121:ATFTSA%3E2.0.CO;2
- 607 Köhl A (2005) Anomalies of Meridional Overturning: Mechanisms in the North Atlantic.
608 *Journal of Physical Oceanography* 35(8):1455–1472, doi:10.1175/JPO2767.1
- 609 Kang SM, Frierson DMW, Held IM (2009) The Tropical Response to Extratropical Thermal
610 Forcing in an Idealized GCM: The Importance of Radiative Feedbacks and Convective
611 Parameterization. *Journal of the Atmospheric Sciences* 66:2812–2827
- 612 Kawase M (1987) Establishment of Deep Ocean Circulation Driven by Deep-Water
613 Production. *Journal of Physical Oceanography* 17(12):2294–2317, doi:10.1175/1520-
614 0485(1987)017%3C2294:EODOCD%3E2.0.CO;2
- 615 Keenlyside NS, Latif M, Jungclauss J, Kornblueh L, Roeckner E (2008) Advancing decadal-
616 scale climate prediction in the North Atlantic sector. *Nature* 453(7191):84–88, doi:
617 10.1038/nature06921
- 618 Knight JR, Allan RJ, Folland CK, Vellinga M, Mann ME (2005) A signature of persistent
619 natural thermohaline circulation cycles in observed climate. *Geophysical Research Letters*
620 32(20):L20,708+, doi:10.1029/2005GL024233
- 621 Knight JR, Folland CK, Scaife AA (2006) Climate impacts of the Atlantic Multidecadal Os-
622 cillation. *Geophysical Research Letters* 33(17):L17,706+, doi:10.1029/2006GL026242
- 623 Marshall J, Schott F (1999) Open-ocean convection: Observations, theory, and models. *Re-
624 views of Geophysics* 37(1):null–64, doi:10.1029/98RG02739
- 625 Palter JB, Lozier MS, Lavender KL (2008) How Does Labrador Sea Water En-
626 ter the Deep Western Boundary Current? *J Phys Oceanogr* 38(5):968–983, doi:
627 10.1175/2007JPO3807.1
- 628 Pohlmann H, Jungclauss JH, Köhl A, Stammer D, Marotzke J (2009) Initializing Decadal
629 Climate Predictions with the GECCO Oceanic Synthesis: Effects on the North Atlantic. *J
630 Climate* 22(14):3926–3938, doi:10.1175/2009JCLI2535.1
- 631 Robson J, Sutton R, Lohmann K, Smith D, Palmer M (2011) Causes of the rapid warming
632 of the north atlantic ocean in the mid 1990s. *J Climate*
- 633 Roussenov VM, Williams RG, Hughes CW, Bingham RJ (2008) Boundary wave commu-
634 nication of bottom pressure and overturning changes for the North Atlantic. *Journal of
635 Geophysical Research* 113:C08,042+, doi:10.1029/2007JC004501
- 636 Schwab D (1998) Propagation of Kelvin waves along irregular coastlines in finite-
637 difference models. *Advances in Water Resources* 22(3):239–245, doi:10.1016/S0309-
638 1708(98)00015-3
- 639 Shaffrey LC, Stevens I, Norton WA, Roberts MJ, Vidale PL, Harle JD, Jrrar A, Stevens
640 DP, Woodage MJ, Demory ME, Donners J, Clark DB, Clayton A, Cole JW, Wilson
641 SS, Connolley WM, Davies TM, Iwi AM, Johns TC, King JC, New AL, Slingo JM,
642 Slingo A, Steenman-Clark L, Martin GM (2009) U.K. HiGEM: The New U.K. High-
- 643

- 644 Resolution Global Environment Model Model Description and Basic Evaluation. *J Cli-*
645 *mate* 22(8):1861–1896, doi:10.1175/2008JCLI2508.1
- 646 Shaw PT, Csanady GT (1983) Self-Advection of Density Perturbations on a Sloping
647 Continental Shelf. *Journal of Physical Oceanography* 13(5):769–782, doi:10.1175/1520-
648 0485(1983)013%3C0769:SAODPO%3E2.0.CO;2
- 649 Smith DM, Cusack S, Colman AW, Folland CK, Harris GR, Murphy JM (2007) Improved
650 Surface Temperature Prediction for the Coming Decade from a Global Climate Model.
651 *Science* 317(5839):796–799, doi:10.1126/science.1139540
- 652 Smith RS, Gregory JM (2009) A study of the sensitivity of ocean overturning circulation
653 and climate to freshwater input in different regions of the North Atlantic. *Geophysical*
654 *Research Letters* 36(15):L15,701+, doi:10.1029/2009GL038607
- 655 Sutton R, Hodson D (2005) Atlantic ocean forcing of north american and european summer
656 climate. *Science* 309:115–118
- 657 Sutton R, Hodson D (2007) Climate response to a multidecadal warming and cooling of the
658 north atlantic ocean. *J Climate* 20(5):891–907
- 659 Sutton R, Jewson S, Rowell D (2000) The elements of climate variability in the tropical
660 atlantic region. *J Climate* 13:3261–3284
- 661 Terray L, Cassou C (2002) Tropical atlantic sea surface temperature forcing of quasi-decadal
662 climate variability over the north atlantic-europe region. *J Climate* 15(22):3170–3187
- 663 Trenberth KE, Caron JM (2001) Estimates of Meridional Atmosphere and Ocean
664 Heat Transports. *Journal of Climate* 14(16):3433–3443, doi:10.1175/1520-
665 0442(2001)014%3C3433:EOMAAO%3E2.0.CO;2
- 666 Vellinga M, Wu P (2004) Low-Latitude Freshwater Influence on Centennial Variability of
667 the Atlantic Thermohaline Circulation. *Journal of Climate* 17(23):4498–4511
- 668 Vellinga M, Wood RA, Gregory JM (2002) Processes Governing the Recovery of a Per-
669 turbed Thermohaline Circulation in HadCM3. *Journal of Climate* 15(7):764–780, doi:
670 10.1175/1520-0442(2002)015%3C0764:PGTROA%3E2.0.CO;2
- 671 Wunsch C, Heimbach P (2006) Estimated Decadal Changes in the North Atlantic Meridional
672 Overturning Circulation and Heat Flux 1993–2004. *Journal of Physical Oceanog-*
673 *raphy* 36(11):2012–2024, doi:10.1175/JPO2957.1
- 674 Zhang D, Msadek R, McPhaden MJ, Delworth T (2011) Multidecadal variability of the
675 North Brazil Current and its connection to the Atlantic meridional overturning circulation.
676 *Journal of Geophysical Research* 116(C4):C04,012+, doi:10.1029/2010JC006812
- 677 Zhang R (2008) Coherent surface-subsurface fingerprint of the Atlantic meridional overturn-
678 ing circulation. *Geophysical Research Letters* 35:L20,705+, doi:10.1029/2008GL035463
- 679 Zhang Z, Kang SM, Held IM (2010) Sensitivity of Climate Change Induced by the Weak-
680 ening of the Atlantic Meridional Overturning Circulation to Cloud Feedback. *Journal of*
681 *Climate* 23:378–389

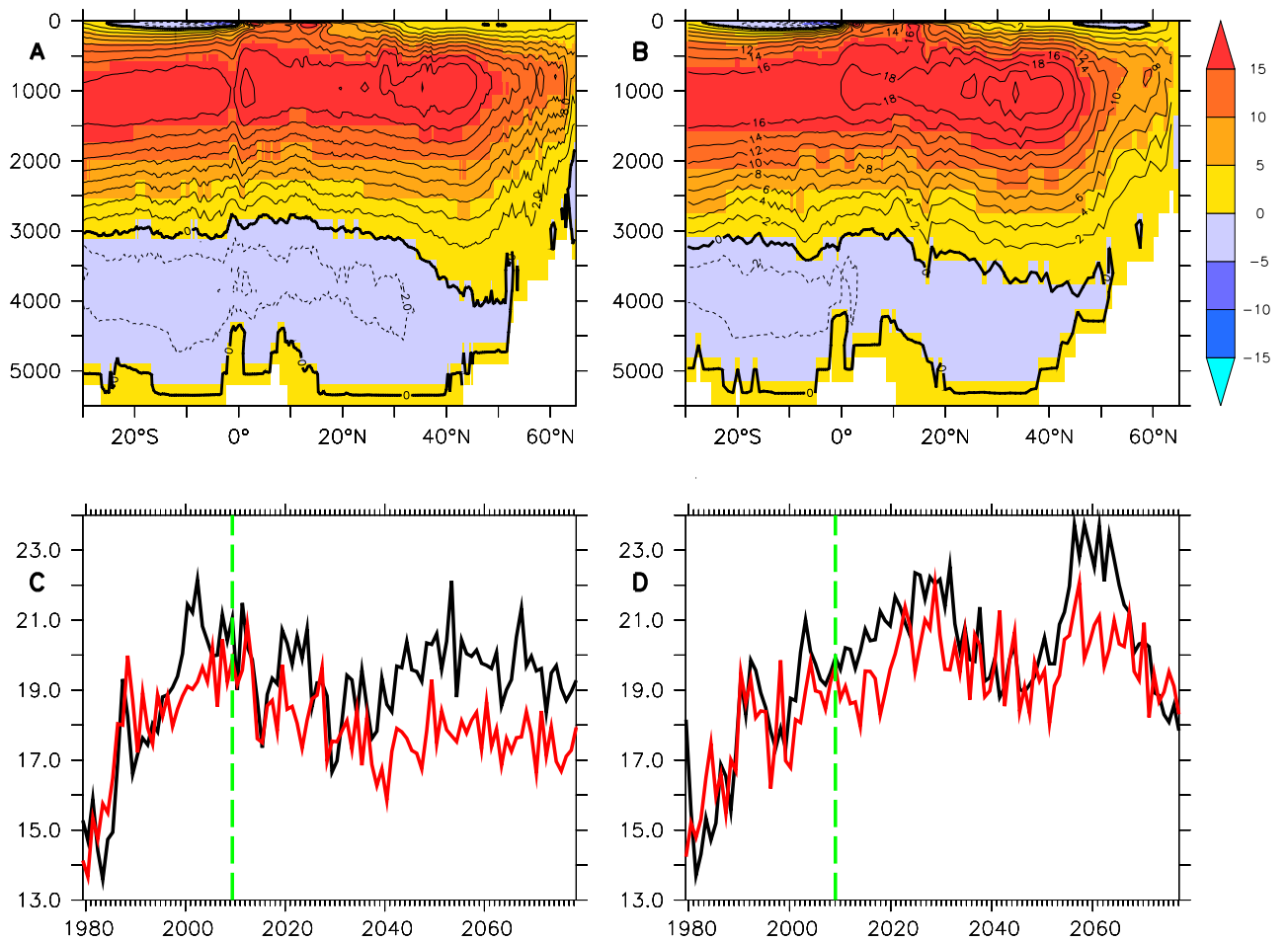


Fig. 1 Annual mean Atlantic meridional stream function (2009:2078, meridional velocity integrated from the ocean floor to a given depth) for A) HiGEM1.2 B) HadGEM1.2. C) Black line: MOC at 40N (meridional ocean velocity integrated across Atlantic basin and from ocean floor to 1000m depth) in HiGEM1.2. Red line: Max Annual mean Atlantic meridional overturning streamfunction (i.e. panel A) at 26.7N in HiGEM1.2. Mean depth of max is 923m for all years. D) as C, but for HadGEM1.2. Mean depth of max is 949m for all years. All units are Sv ($10^6 m^3/s$). Green dotted line denotes 2009. All subsequent analysis is performed on data from 2009 to 2078 (unless otherwise stated) in order to exclude the initial rapid 30 year re-adjustment.

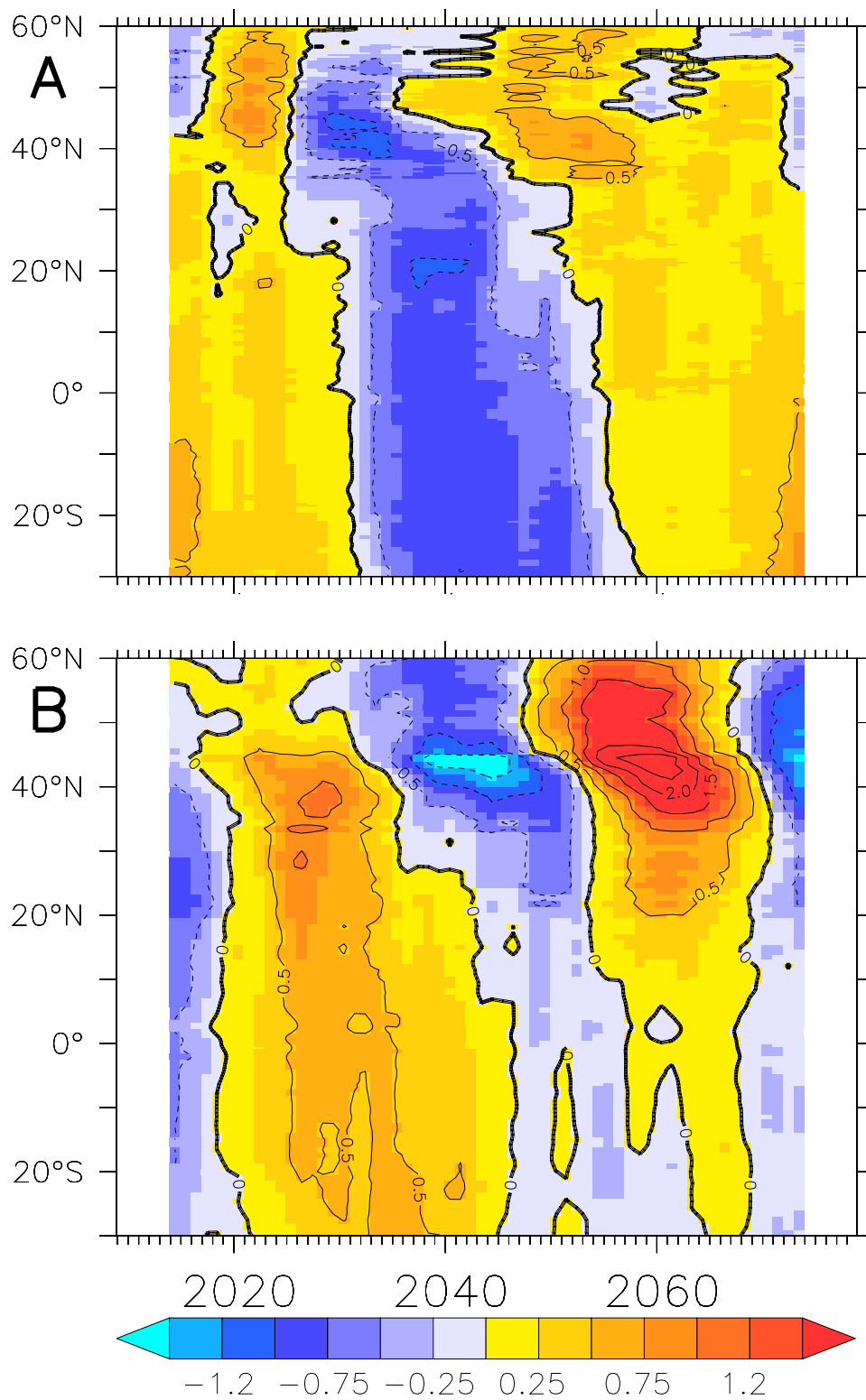


Fig. 2 A) Variation of annual mean HiGEM1.2 MOC (meridional ocean velocity integrated across Atlantic basin and from ocean floor to 1000m depth) with latitude. Only the last 70 years of the 100 year integration were used in this analysis (2009:2078 see Fig. 1). Data from the remaining 70 years of has been detrended and then smoothed with a 10 year running mean time filter. B) as A, but for HadGEM1.2. Units are Sv.

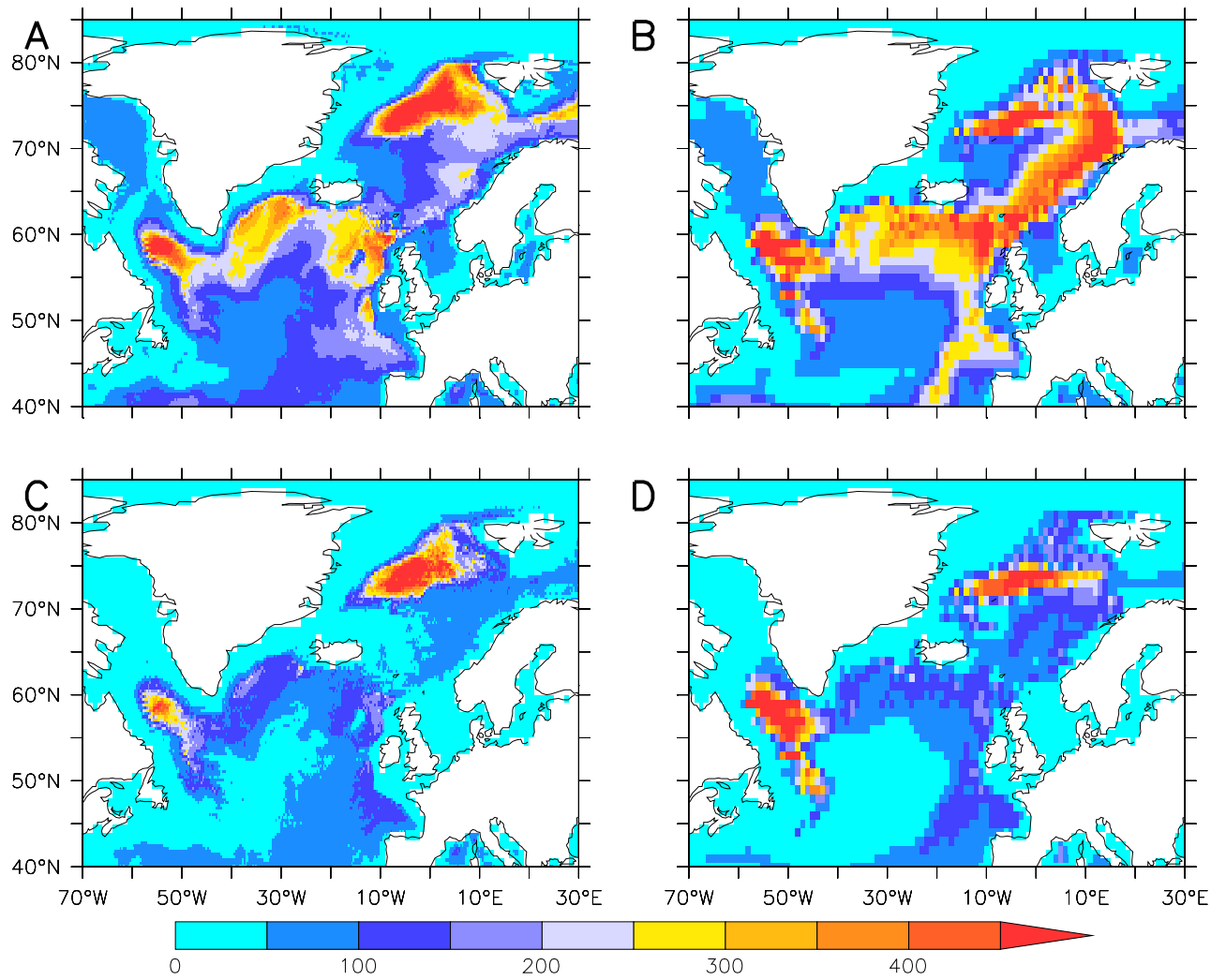


Fig. 3 A) HiGEM1.2 March mean ocean mixed layer depth (2009:2078). B) As A for HadGEM1.2. C) HiGEM1.2 March standard deviation of ocean mixed layer depth (2009:2078). D) As C for HadGEM1.2. Units are m.

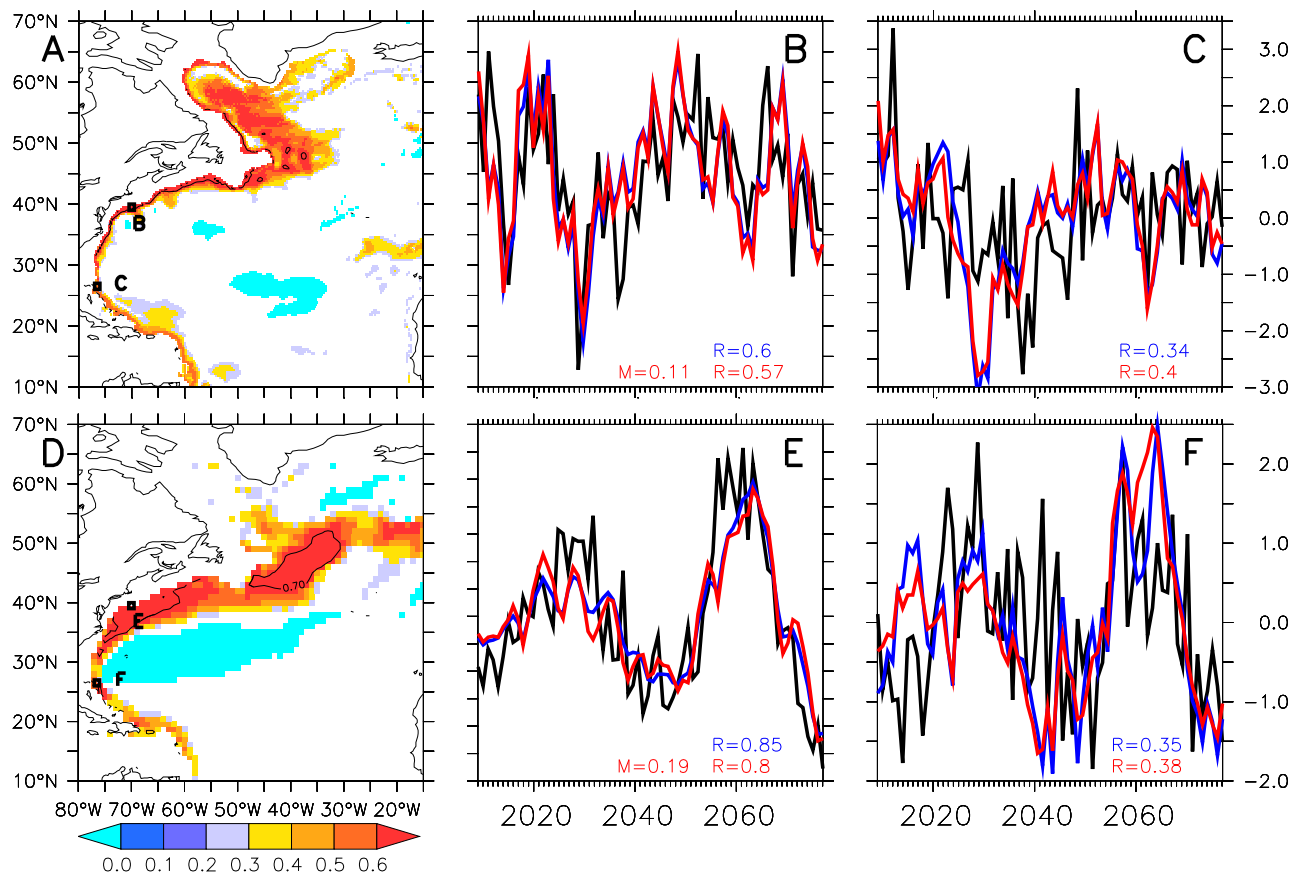


Fig. 4 A) HiGEM1.2 integrated Ocean density (1500-3000m) correlated with integrated density index at point B (MOC^* see panel B: red line). Correlation of 0.7 is contoured. B) Black line: detrended MOC index (as Fig 1C) at 40N. Red Line: index of Detrended (years 31-100), box-averaged (70.5:69.5W,39:40N, box labelled B, in panel A, MOC^*) ocean density, integrated between 1500 and 3000m. Blue line: as Red line but for *double* integrated ocean density, as described in equation C) Black line: detrended MOC index (as Fig 1C) at 26.7N. Red Line: index of Detrended (years 31-100), box-averaged (77:76W,26:27N, box labelled C, in panel A) ocean density, integrated between 1500 and 3000m. Blue line: as Red line but for *double* integrated ocean density, as described in equation All indices in B and C have been *standardized* before plotting. E-F) As A-C, but for HadGEM1.2. Correlation coefficients between MOC (black) and Integrated Density (red) indices are given in **red** in the bottom right hand corner of each panel. Correlation coefficients (**R**) between MOC (black) and Doubly Integrated Density (blue) indices are given in **blue** in the bottom right hand corner of each panel. Regression coefficients (**M**) between MOC^* (red) and MOC (black) (before standardization) are also given in the bottom right hand corner of panels B and E (Units $Sv/(kg/m^2)$).

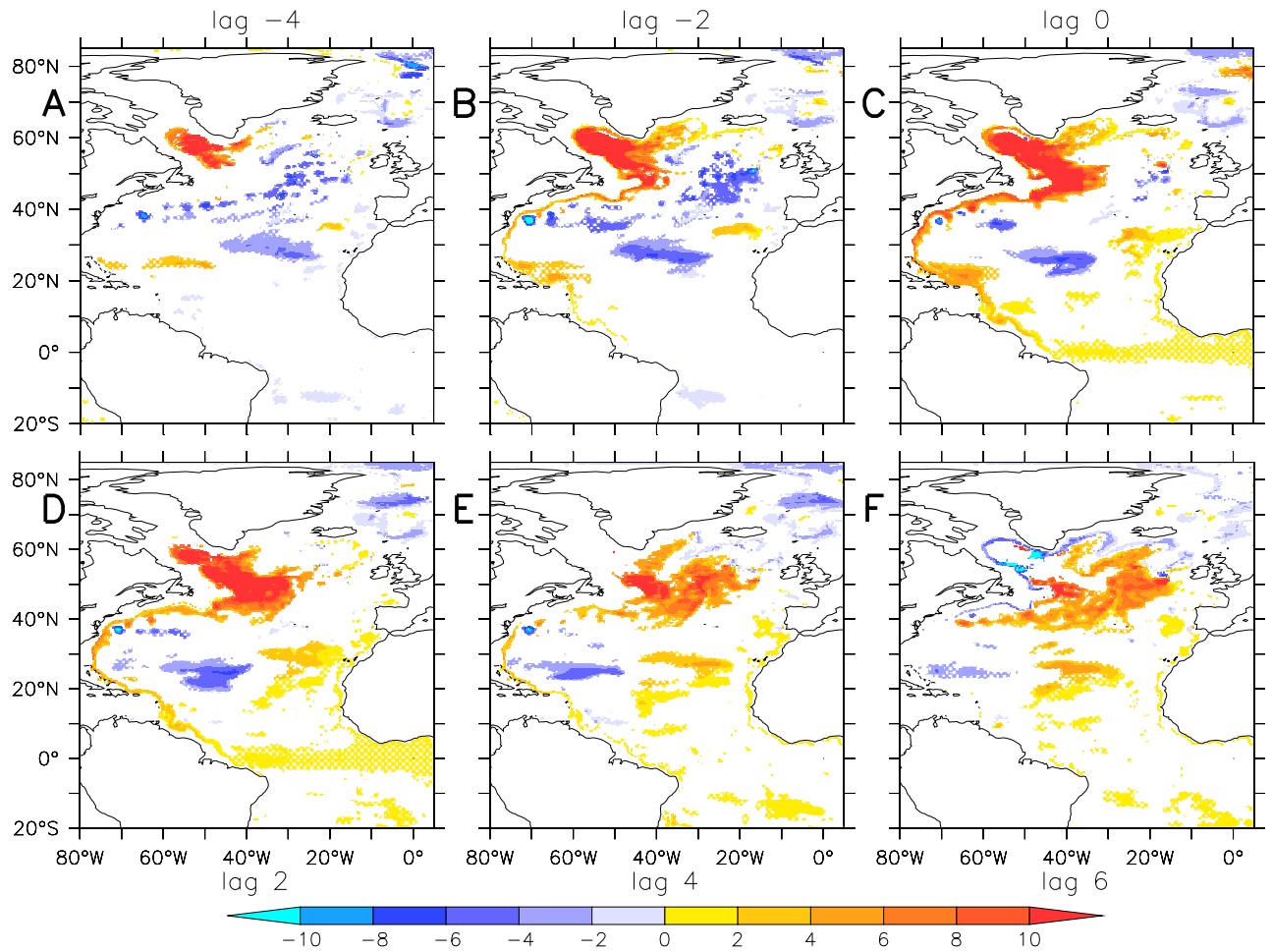


Fig. 5 Annual mean HiGEM1.2 ocean density integrated between 1500m and 3000m then lag regressed onto MOC* - a detrended MOC-proxy index at 40N (see Fig. 4). The ocean Lags the MOC* index for positive lags. Only the last 70 years of the 100 year integration were used in this analysis (2009-2078) (see Figure 1). Here we have multiplied MOC* by the regression value from Figure 4b ($M=0.11 \text{ Sv}/(\text{kg m}^{-2})$) beforehand. Hence the units are $\text{kg m}^{-2}/\text{Sv}$. Regions where the regression is significant ($p < 0.05$) are solid shaded. Regions where ($0.05 \leq p < 0.10$) are stippled shading.

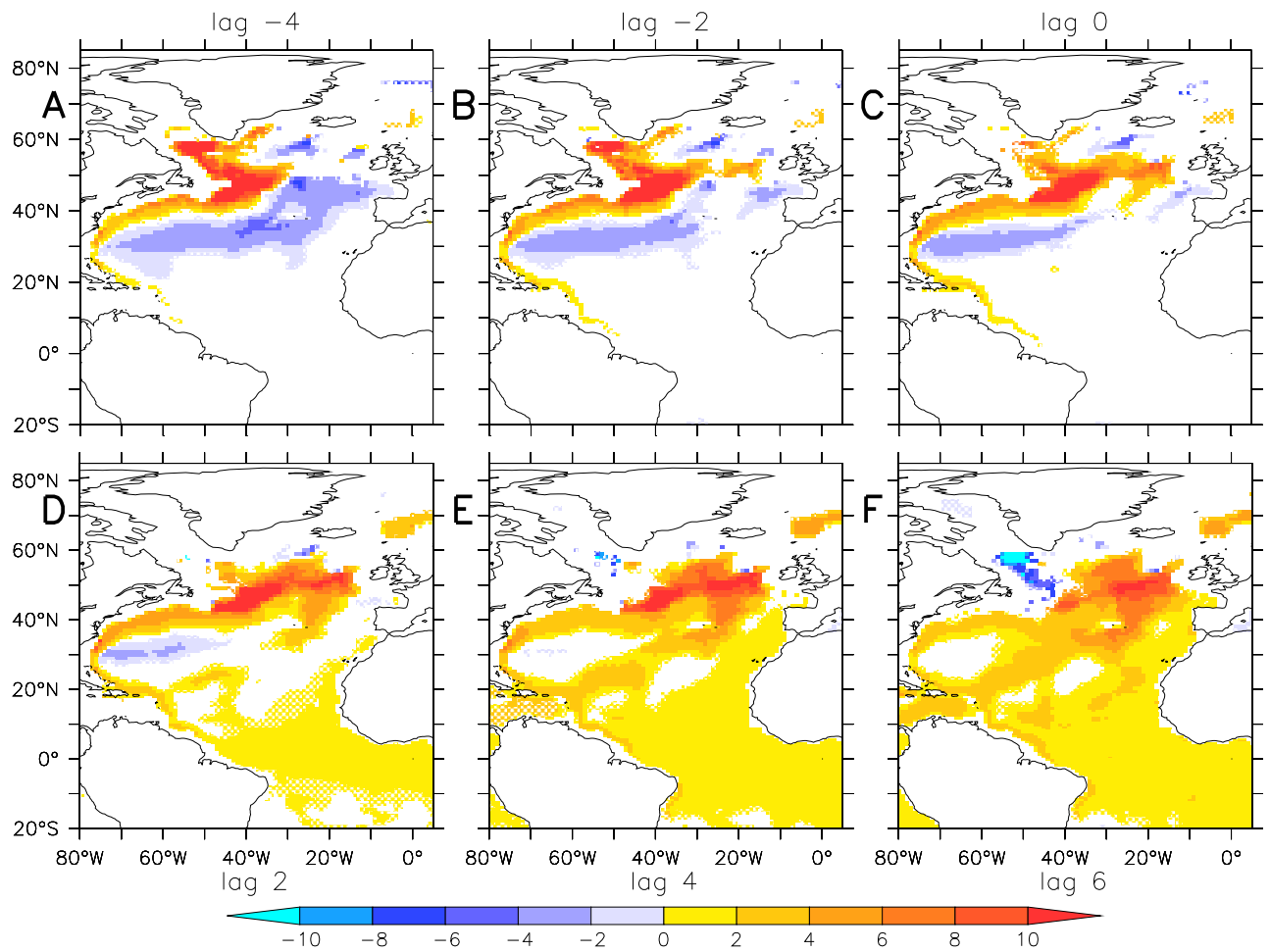


Fig. 6 As Figure 5 but for HadGEM1.2. Here we have multiplied MOC^* by the regression value from Figure 4b ($M=0.18 \text{ Sv}/(\text{kg m}^{-2})$) beforehand. Hence the units are $\text{kg m}^{-2}/\text{Sv}$.

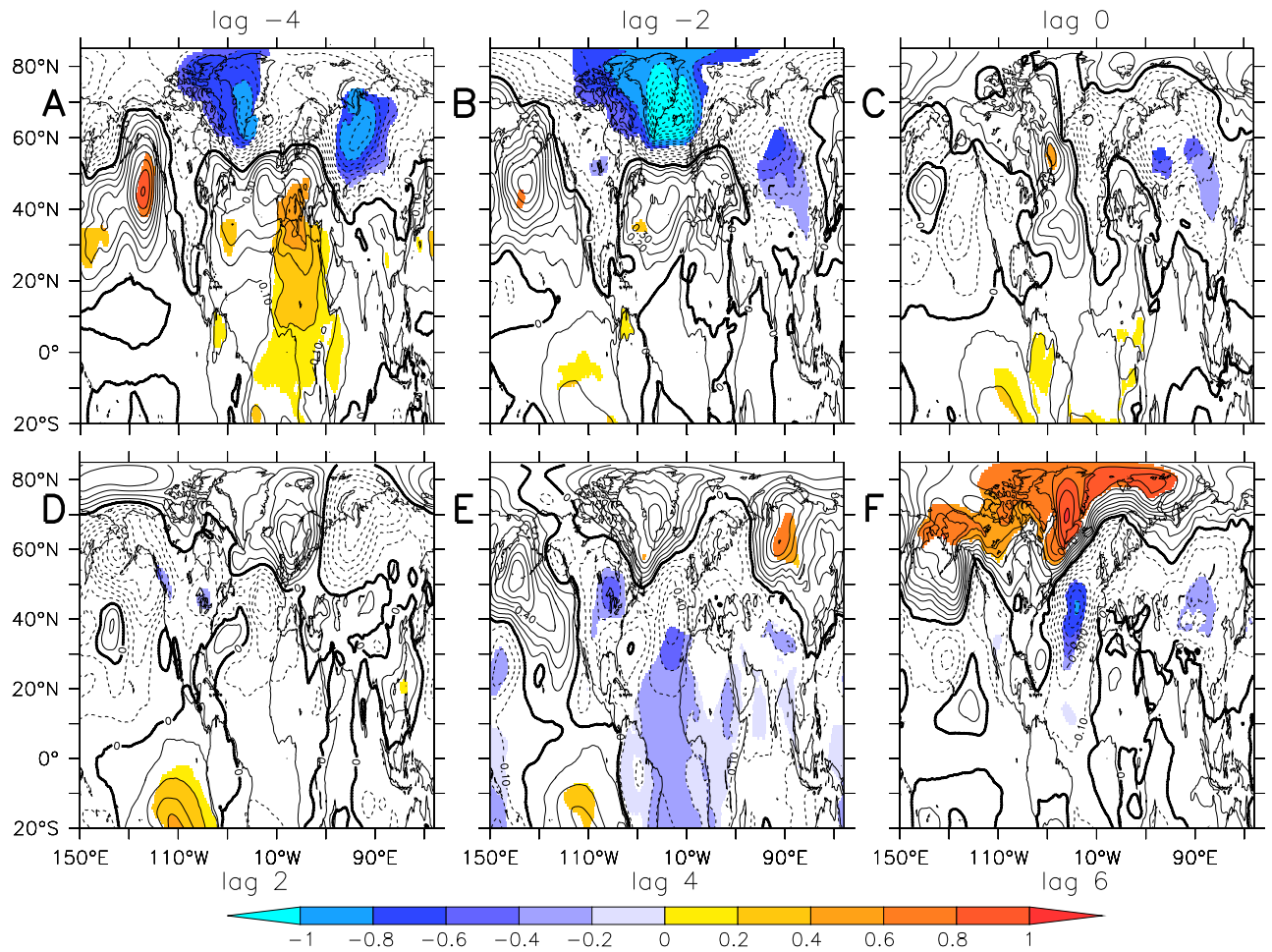


Fig. 7 Annual mean Mean Sea Level Pressure (MSLP) regressed on MOC*, the detrended boundary density index at 40N defined in Figure 4. MSLP field lags boundary index (Hence MOC) for positive lags. As before we have multiplied MOC* by 0.11 ($\text{Sv}/(\text{kg m}^{-2})$) beforehand. Hence the units are hPa/Sv. Regions where the regression is significant ($p < 0.05$) are solid shaded.

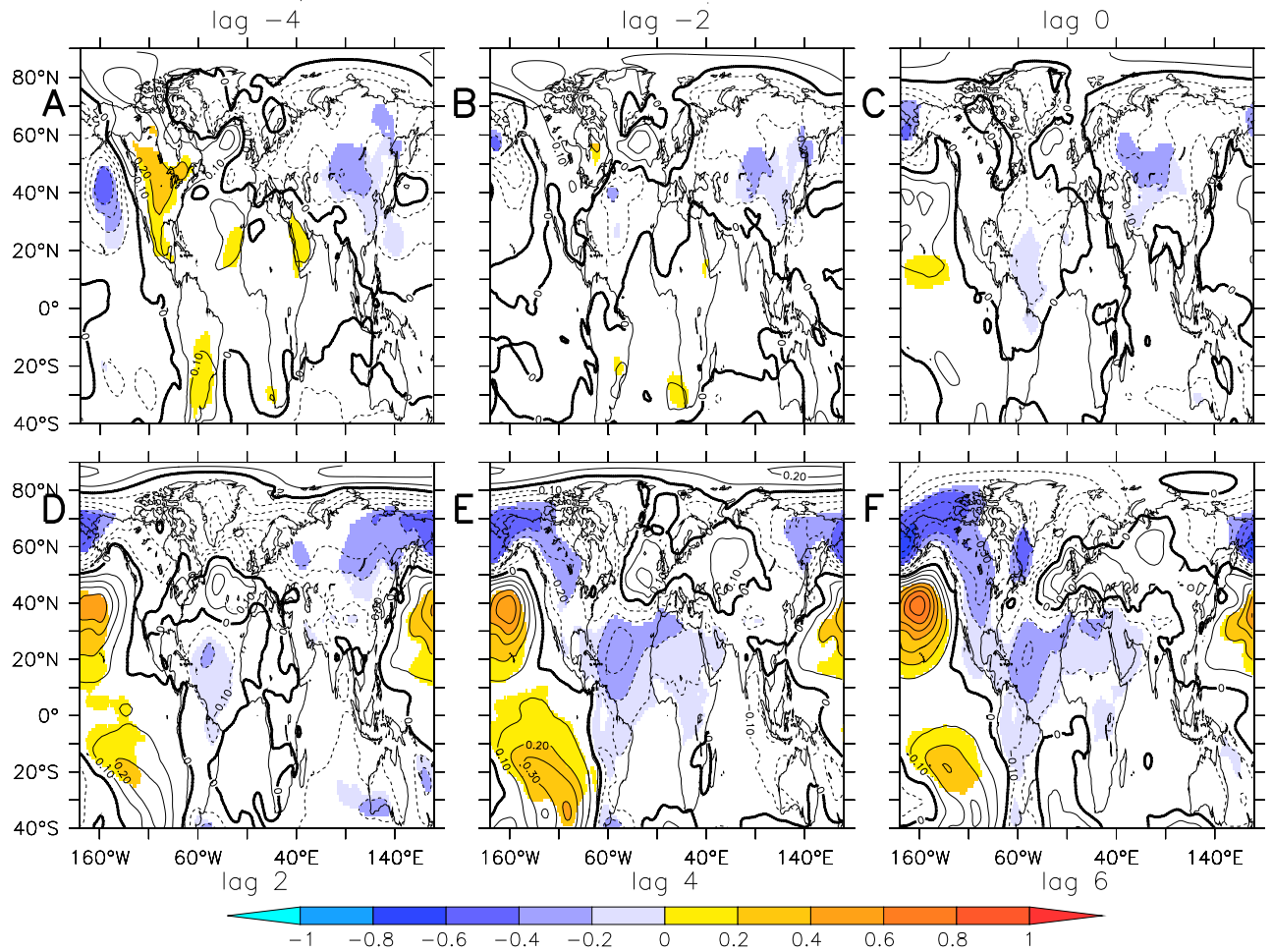


Fig. 8 As Figure 7 but for HadGEM1.2. As before we have multiplied MOC* by 0.18 ($\text{Sv}/(\text{kg m}^{-2})$) beforehand. Hence the units are hPa/Sv .

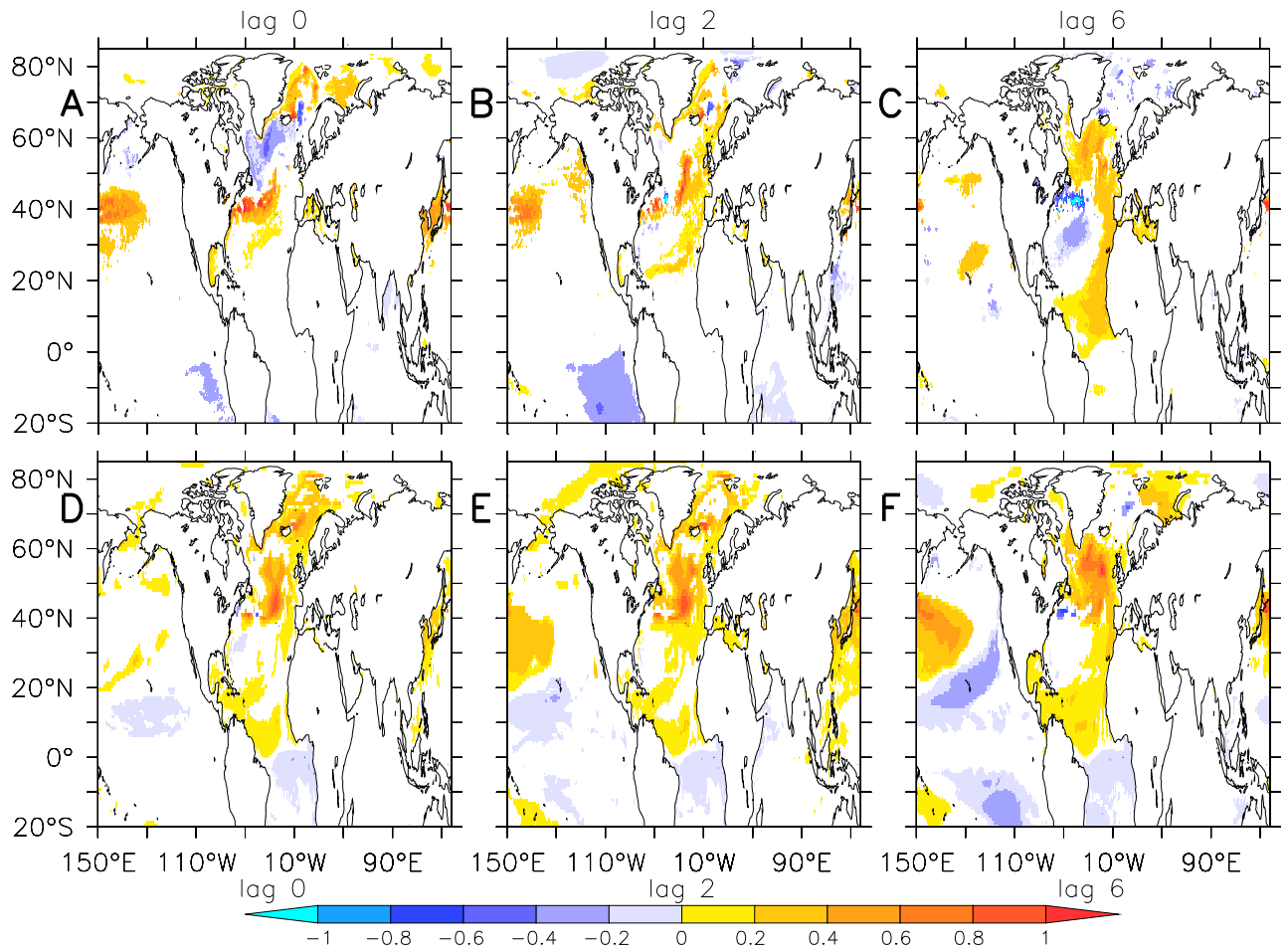


Fig. 9 As Figure 7 but for Sea Surface Temperatures (SSTs). A-C) HiGEM1.2. D-F) HadGEM1.2. MOC* has been scaled appropriately as before. Hence units are K/Sv.

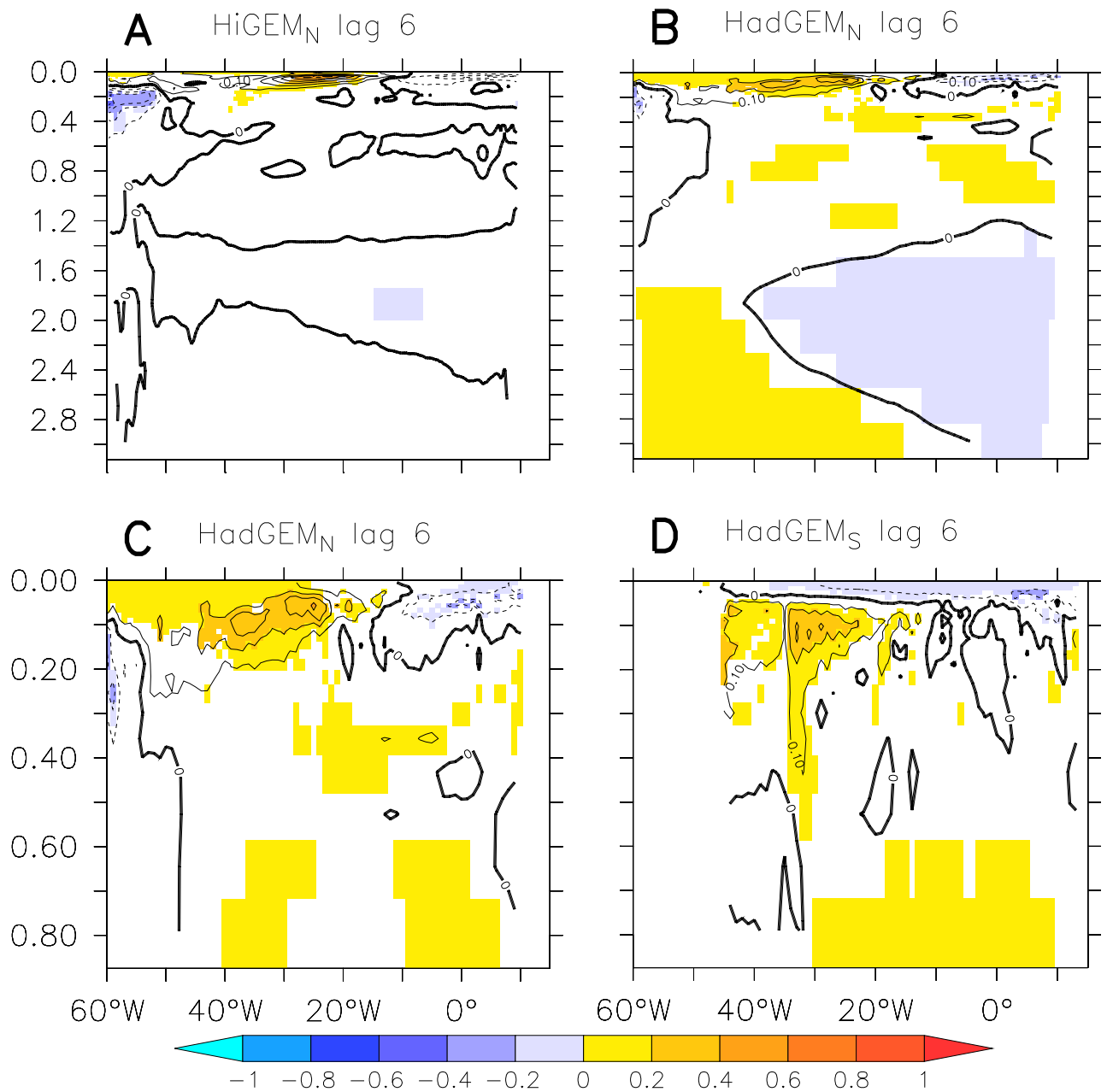


Fig. 10 Tropical Atlantic Ocean temperatures. a) HiGEM1.2 Ocean temperatures averaged between 0:10N lag regressed on the detrended boundary density index at 40N (B in Fig 4a, defined as MOC* in text). Plot shows ocean temperatures six years after an increase in MOC*. MOC* has been scaled appropriately as before. Hence units are K/Sv. b) as a) but for HadGEM1.2. c) An expanded version of b) to show the upper ocean warming. d) as c) but for 0:10S. Units on vertical axes are km.

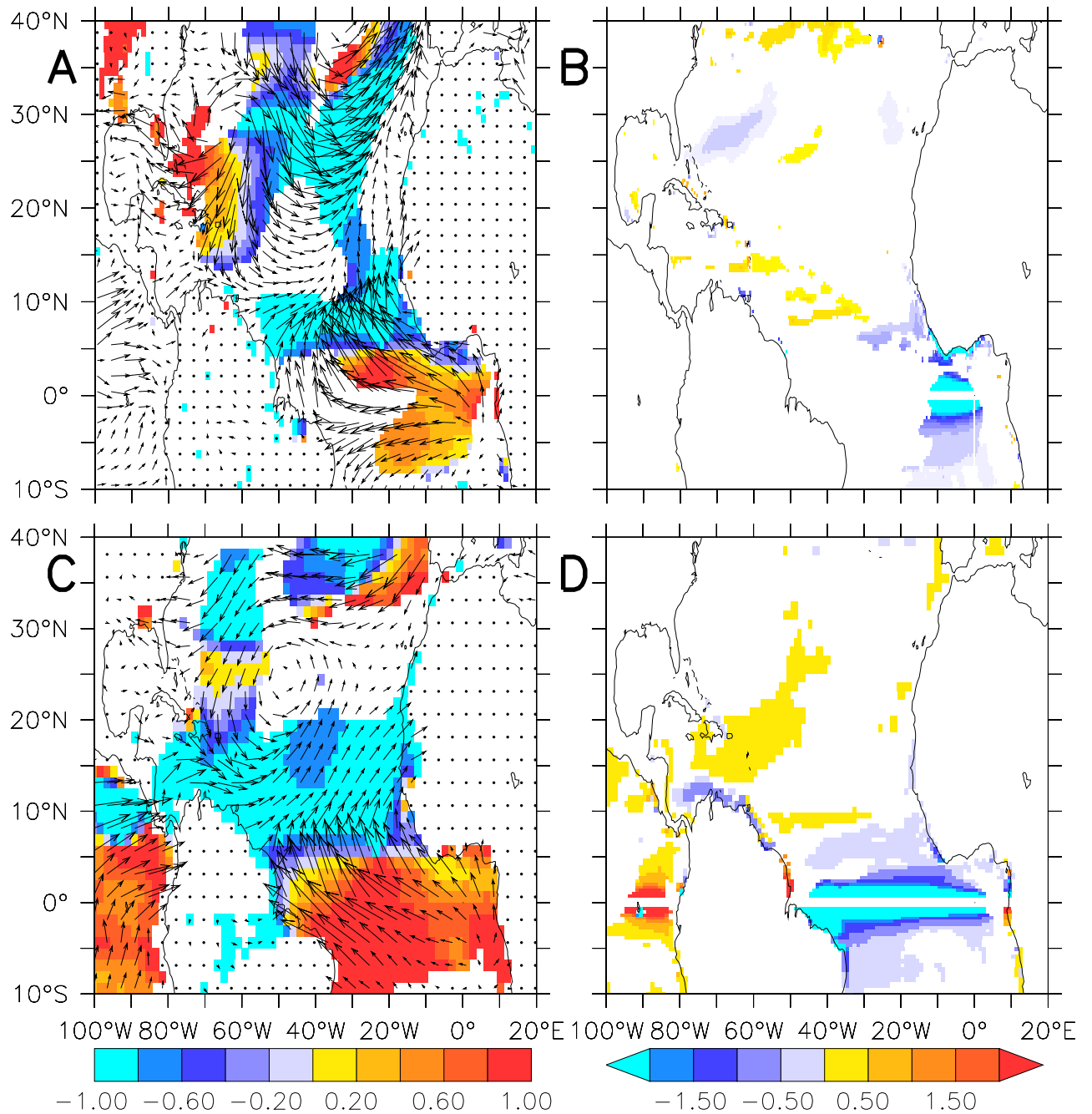


Fig. 11 Surface Winds and Ekman Pumping. a) HiGEM1.2 Surface winds lag regressed onto the detrended boundary density index (MOC^*) at 40N at Lag 6. Plot shows surface wind anomalies six years after an increase in MOC^* . The shading shows the scalar product of the normalized wind anomalies with the normalized mean climatological wind at a grid point (i.e the cosine of the angle between these two vectors). Hence regions where the anomalous wind weakens (strengthens) the mean winds, leading to reduced (enhanced) surface cooling, are shaded blue (red). Only regions where the magnitude of the regression is significant ($p < 0.05$) are shaded. b) HiGEM1.2 Ekman pumping, computed from surface wind stress curl, lag regressed onto the detrended boundary density index (MOC^*) at 40N at Lag 6. Regions where the regression is significant ($p < 0.05$) are shaded. The region between 0.5S and 0.5N is masked out, because the expression for calculating Ekman pumping diverges near the equator. MOC^* has been scaled appropriately as before. Hence, units are $10^{-6} \text{ ms}^{-1}/\text{Sv}$ c) as a) but for HadGEM1.2. d) as b) but for HadGEM1.2.

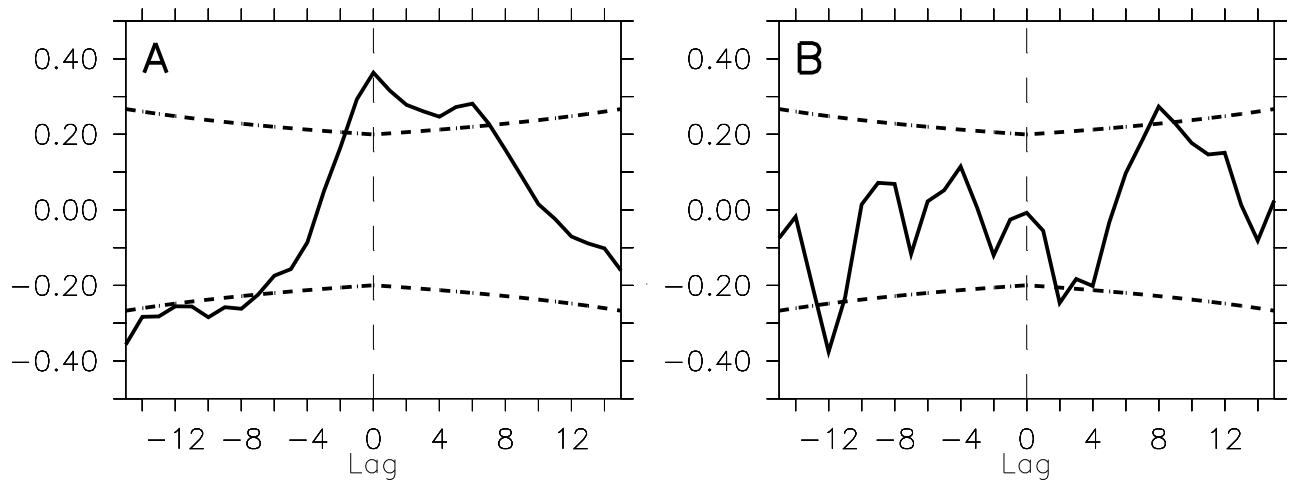


Fig. 12 A) Lag correlation of an index of the North Brazil Current (NBC) and MOC* in HadGEM1.2. MOC* leads for positive lags. Dotted lines indicate significant correlation level ($p < 0.05$). B) as A) but for HiGEM1.2.